Sp(2N) Yang-Mills theories on the lattice: Scale setting and topology

Bennett, Ed; Hong, Deog Ki; Lee, Jong Wan; Lin, C. J.David; Lucini, Biagio; Piai, Maurizio; Vadacchino, Davide

Published in:
Physical Review D

DOI:
10.1103/physrevd.106.094503

Publication date:
2022

$Sp(2N)$ Yang-Mills theories on the lattice: Scale setting and topology

Ed Bennett,[1,*] Deog Ki Hong,[2,†] Jong-Wan Lee,[2,3,‡] C.-J. David Lin,[4,5,6,7,§] Biagio Lucini,[8,1,‖] Maurizio Piai,[9,¶] and Davide Vadacchino[10,11,**]

[1]*Swansea Academy of Advanced Computing, Swansea University, Fabian Way, SA1 8EN Swansea, Wales, United Kingdom*
[2]*Department of Physics, Pusan National University, Busan 46241, Republic of Korea*
[3]*Institute for Extreme Physics, Pusan National University, Busan 46241, Republic of Korea*
[4]*Institute of Physics, National Yang Ming Chiao Tung University, 1001 Ta-Hsueh Road, Hsinchu 30010, Taiwan*
[5]*Center for High Energy Physics, Chung-Yuan Christian University, Chung-Li 32023, Taiwan*
[6]*Centre for Theoretical and Computational Physics, National Yang Ming Chiao Tung University, 1001 Ta-Hsueh Road, Hsinchu 30010, Taiwan*
[7]*Physics Division, National Centre for Theoretical Sciences, Taipei 10617, Taiwan*
[8]*Department of Mathematics, Faculty of Science and Engineering, Swansea University, Fabian Way, SA1 8EN Swansea, Wales, United Kingdom*
[9]*Department of Physics, Faculty of Science and Engineering, Swansea University, Singleton Park, SA2 8PP Swansea, Wales, United Kingdom*
[10]*School of Mathematics and Hamilton Mathematics Institute, Trinity College, Dublin 2, Ireland*
[11]*Centre for Mathematical Sciences, University of Plymouth, PL4 8AA Plymouth, United Kingdom*

(Received 25 June 2022; accepted 3 October 2022; published 15 November 2022)

We study Yang-Mills lattice theories with $Sp(N_c)$ gauge group, with $N_c = 2N$, for $N = 1, \ldots, 4$. We show that if we divide the renormalized couplings appearing in the Wilson flow by the quadratic Casimir $C_2(F)$ of the $Sp(N_c)$ group, then the resulting quantities display a good agreement among all values of N_c considered, over a finite interval in flow time. We use this scaled version of the Wilson flow as a scale-setting procedure, compute the topological susceptibility of the $Sp(N_c)$ theories, and extrapolate the results to the continuum limit for each N_c.

DOI: 10.1103/PhysRevD.106.094503

I. INTRODUCTION

Lattice studies of $Sp(N_c = 2N)$ gauge theories aim at quantitatively appraising, in the strong coupling regime, what their distinctive features are in respect to theories based upon $SU(N_c)$ gauge groups. For example, a long list of recent investigations of the $SU(2) \sim Sp(2)$ theories [1–9], and of the $Sp(2N)$ theories for $N > 1$ [10–17], are motivated by their paradigm changing potential for applications in contemporary high energy physics.

Prominently, enhanced global symmetry and symmetry breaking patterns arise in $Sp(2N)$ theories in the presence of matter fields. This feature is exploited in new-physics model-building exercises such as in the minimal model in Ref. [18], which combines a composite Higgs model (CHM)—in which the Higgs fields originate as pseudo-Nambu-Goldstone bosons (PNGBs) in a new strongly coupled sector [19–21]—with partial top compositeness [22]. For recent reviews see Refs. [23–25], and the summary tables in Refs. [26–28]. In the different context of dark matter models emerging from strongly coupled dynamics [29–32], $Sp(2N)$ gauge theories have also been attracting increasing interest [33–40].

There are more general, theoretical reasons to study $Sp(2N)$ gauge theories. Pioneering studies of the pure gauge cases [41] aimed at qualifying the role of the center symmetry in the confinement/deconfinement transition at finite temperature. In the light of the conjectured existence of dualities between large-N_c gauge theories and theories of gravity in higher dimension [42–45], the appeal of $Sp(N_c)$ theories derives from the common features that they share with $SU(N_c)$ theories. For example, extensive

*e.j.bennett@swansea.ac.uk
†dkhong@pusan.ac.kr
‡jwlee823@pusan.ac.kr
§dlin@nycu.edu.tw
‖b.lucini@swansea.ac.uk
¶m.piai@swansea.ac.uk
**davide.vadacchino@plymouth.ac.uk

studies of the spectrum of glueballs and strings confirm that universal features emerge at large N_c, common to $SU(N_c)$, $Sp(N_c)$, and $SO(N_c)$ theories [14,15,46–56].

The topological susceptibility, χ (to be defined in the body of the paper), plays a central role in our understanding of QCD, for several intercorrelated reasons of historical significance. It enters the Witten-Veneziano formula [57,58] for the large-N_c behavior of the mass of the η' meson, and the solution to the $U(1)_A$ problem. Allowing the gauge coupling to be complex, and expanding in powers of (small) θ, χ appears as the coefficient at $O(\theta^2)$ in the free energy. Indirectly, it might hence have implications for the strong-CP problem, for the physics of putative new particles such as the axion, and for the electric dipole moments of hadrons. Many interesting lattice calculations of χ exist—see Refs. [46,55,59–71], and Tables I and II of the review in Ref. [72].

Accounting for χ might provide new insight in the role of instantons and other nonperturbative objects. A precise knowledge of χ might have unexpectedly important consequences also in the aforementioned subfield encompassing modern phenomenological applications of strongly -coupled $Sp(N_c)$ theories—models of composite Higgs, partial top compositeness, dark matter, or even early Universe physics. In general, precise calculations of χ might sharpen our understanding both of commonalities and differences between $Sp(N_c)$ and $SU(N_c)$ theories, starting in the Yang-Mills (pure gauge) theories.

Motivated by such considerations, and as an important step in the program of study of $Sp(N_c)$ lattice gauge theories conducted by our collaboration, in this paper we compute the topological susceptibility of $Sp(N_c)$ Yang-Mills theories for $N_c \leq 8$. We made available preliminary results in contributions to conference proceedings [73,74], but this analysis is much improved, and based on larger statistics. In a dedicated publication, we compare our results for $Sp(N_c)$ with the $SU(N_c)$ literature, and discuss the large-N_c extrapolation [75].

The paper is organized as follows. In Sec. II we define the lattice theories of interest. In Sec. III we discuss how to use the gradient flow and its lattice implementation, the Wilson flow [76,77], as a scale-setting procedure, and define the topological charge and susceptibility. Section IV is the main body of the paper, in which we present our numerical results. We conclude with the summary in Sec. V. We relegate some useful details to the Appendix.

II. $Sp(2N)$ YANG-MILLS THEORIES

We define the continuum $Sp(2N)$ gauge theories, in 4-dimensional Euclidean space, in terms of the action

$$S_{\rm YM} \equiv -\frac{1}{2g_0^2}\int \mathrm{d}^4x \mathrm{Tr} F_{\mu\nu}F^{\mu\nu}, \tag{1}$$

where g_0 is the gauge coupling, $F_{\mu\nu} \equiv \sum_A F^A_{\mu\nu}\tau^A$, with

$$F^A_{\mu\nu} = \partial_\mu A^A_\nu - \partial_\nu A^A_\mu + f^{ABC}A^B_\mu A^C_\nu, \tag{2}$$

and the trace is over the color index on the fundamental representation, while $A = 1, \ldots, N(2N+1)$. The Hermitian matrices $\tau^A \in \mathbb{C}^{2N\times 2N}$ are the generators of the algebra associated to the Lie group $Sp(2N)$ in the fundamental representation. They satisfy the relations

$$[\tau^A, \tau^B] = if^{ABC}\tau^C, \tag{3}$$

and are normalized according to $\mathrm{Tr}(\tau^A\tau^B) = \frac{1}{2}\delta^{AB}$.

The configuration space of this theory can be partitioned into sectors, characterized by the value of the *topological charge* Q, defined as follows:

$$Q \equiv \int \mathrm{d}^4x q(x), \tag{4}$$

where

$$q(x) \equiv \frac{1}{32\pi^2}\epsilon^{\mu\nu\rho\sigma}\mathrm{Tr}F_{\mu\nu}(x)F_{\rho\sigma}(x). \tag{5}$$

The *topological susceptibility*, χ, is defined as

$$\chi \equiv \int \mathrm{d}^4x \langle q(x)q(0)\rangle. \tag{6}$$

The possible values of Q belong to the third homotopy group of the gauge group. Since $Sp(2N)$ is compact, connected and simple, one finds that

$$\pi_3(Sp(2N)) = \mathbb{Z}, \tag{7}$$

as in the case of $SU(N_c)$ gauge theories.

A. The lattice

A lattice regularization of the theory defined in Eq. (1) allows us to characterize quantitatively its nonperturbative features. We adopt a 4-dimensional Euclidean hypercubic lattice Λ, with lattice spacing a. The sites of the lattice are denoted by their Cartesian coordinates $x = \{x_\mu\}$ and the links by (x,μ), where $\mu = 0, \ldots, 3$ and $x_\mu = n_\mu a$. For a lattice of length L_μ in the μ directions, with $n_\mu = 0, \ldots, L_\mu/a - 1$, the total number of sites is thus $V_4/a^4 = L_0L_1L_2L_3/a^4$. The lattices used in our calculations are isotropic in the four directions, $L_\mu = L$, and we impose periodic boundary conditions in all directions. The elementary degrees of freedom of the theory are called *link variables*, and defined as

$$U_\mu(x) \equiv \exp\left(i\int_x^{x+\hat{\mu}} \mathrm{d}\lambda^\mu \tau^A A^A_\mu(\lambda)\right), \tag{8}$$

where $\hat{\mu}$ is the unit vector in direction μ. The link variables are $2N \times 2N$ matrices that, under the action of a gauge transformation $g(x) \in Sp(2N)$, transform as

$$U_\mu(x) \to g(x)U_\mu(x)g^\dagger(x+\hat{\mu}). \tag{9}$$

The trace of a path-ordered product of link variables defined along a closed lattice path is hence gauge invariant.

The simplest such closed path on the lattice defines the *elementary plaquette* $\mathcal{P}_{\mu\nu}$:

$$\mathcal{P}_{\mu\nu}(x) \equiv U_\mu(x)U_\nu(x+\hat{\mu})U_\mu^\dagger(x+\hat{\nu})U_\nu^\dagger(x), \tag{10}$$

and is used to define the *Wilson action* $S_{\rm W}$ of the lattice gauge theory:

$$S_{\rm W} \equiv \beta\sum_x\sum_{\mu<\nu}\left(1-\frac{1}{2N}\Re{\rm Tr}\mathcal{P}_{\mu\nu}\right), \tag{11}$$

where the *inverse coupling* β is defined as

$$\beta \equiv \frac{4N}{g_0^2}. \tag{12}$$

Another operator that is useful in lattice calculations is the *clover-leaf plaquette* operator, defined as [78,79]

$$\begin{aligned}\mathcal{C}_{\mu\nu}(x) \equiv \frac{1}{8}\{&U_\mu(x)U_\nu(x+\hat{\mu})U_\mu^\dagger(x+\hat{\nu})U_\nu^\dagger(x)\\ &+U_\nu(x)U_\mu^\dagger(x+\hat{\nu}-\hat{\mu})U_\nu^\dagger(x-\hat{\mu})U_\mu(x-\hat{\mu})\\ &+U_\mu^\dagger(x-\hat{\mu})U_\nu^\dagger(x-\hat{\nu}-\hat{\mu})U_\mu(x-\hat{\nu}-\hat{\mu})U_\nu(x-\hat{\nu})\\ &+U_\nu^\dagger(x-\hat{\nu})U_\mu(x-\hat{\nu})U_\mu(x-\hat{\nu}+\hat{\mu})U_\mu^\dagger(x)-{\rm H.c.}\}.\end{aligned} \tag{13}$$

This operator is used in the literature as a way to improve the Yang-Mills lattice action, particularly in the presence of fermions. In the context of this paper, it serves two purposes: we use it to test the regularization dependence of our scale-setting procedure, but also in the definition of the lattice counterparts of Q and χ.

Vacuum expectation values of operators $\mathcal{O}(U_\mu)$ built of link variables are formally defined as ensemble averages:

$$\langle\mathcal{O}\rangle \equiv \frac{\int\mathcal{D}U_\mu e^{-S_{\rm W}}\mathcal{O}(U_\mu)}{Z(\beta)}, \tag{14}$$

where $\mathcal{D}U_\mu \equiv \prod_{x,\mu}{\rm d}U_\mu(x)$, ${\rm d}U_\mu(x)$ being the Haar measure on $Sp(2N)$, while

$$Z(\beta) \equiv \int\mathcal{D}U_\mu e^{-S_{\rm W}} \tag{15}$$

is the partition function of the system.

For a given value of β and L/a, ensembles are generated by a Markovian process that updates the values of the link variables in a configuration. The updated algorithm must respect detailed balance and have equilibrium distribution $e^{-S_{\rm W}}$. An update of all the links of the lattice is called a *lattice sweep*. It is customary to repeat the update process, subsequent configurations i and $i+1$ in the ensemble being separated by a fixed number $N_{\rm sw}$ of sweeps. The ensemble average takes the simpler form

$$\langle\mathcal{O}\rangle = \lim_{M\to\infty}\sum_{i=1}^{M}\mathcal{O}_i, \tag{16}$$

with $\mathcal{O}_i$ the observable $\mathcal{O}$ evaluated on configuration i. The algorithm we adopt combines local heat bath and overrelaxation updates, implemented in an openly available [80] adaptation of the HiRep code [81] to $Sp(2N)$ groups [15].

The discretized topological charge density can be defined in several different ways [67,82], that differ by terms proportional to a power of a. For the body of this paper, we use the clover-leaf discretization,

$$q_L(x) \equiv \frac{1}{32\pi^2}\epsilon^{\mu\nu\rho\sigma}{\rm Tr}\mathcal{C}_{\mu\nu}(x)\mathcal{C}_{\rho\sigma}(x). \tag{17}$$

Both clover-leaf and elementary plaquette definitions of $q_L(x)$—the latter obtained by replacing $\mathcal{C}_{\mu\nu}(x)$ with $\mathcal{P}_{\mu\nu}$ in Eq. (17)—converge to $q(x)$ in Eq. (5), as $a\to 0$. But the clover-leaf definition treats all lattice directions symmetrically. The (lattice) topological charge is thus

$$Q_L = \sum_x q_L(x), \tag{18}$$

and its susceptibility is

$$\chi_L = \sum_x\langle q_L(x)q_L(0)\rangle. \tag{19}$$

Estimates of physical quantities obtained for given values of β and L/a are affected by several types of systematic errors. Finite size (or volume) effects arise when probing the system over physical distances that are not much smaller than L. This systematic error becomes insignificant if an increase in L/a has an effect that is smaller than statistical fluctuations. Studies of the topology in $SU(N_c)$ gauge theories show that finite size effects are negligible provided $\sqrt{\sigma}L \gtrsim 3$, where σ is the string tension—see, e.g., Figs. 3 and 4 of Ref. [66]. We use earlier analysis of the $Sp(N_c)$ spectrum [15] to identify regions of parameter space satisfying this condition.

The evaluation of χ via lattice methods is particularly challenging, affected by specific systematic effects. First, the configuration space of the lattice theory is simply connected. Topological sectors, and discrete topological charges, are recovered only in the vicinity of the continuum limit [83], while Q_L is not integer, which affects χ_L.

Second, it is challenging to control the continuum extrapolation. χ_L is particularly sensitive to discretization

effects, quantum UV fluctuations yielding both additive and multiplicative renormalization [67,72,82]. We extract χ_L from Wilson-flowed configurations, as we describe in Sec. III, hence adopting a scale-setting procedure that is also used to smoothen out such divergences.

Third, the evaluation of χ_L in $SU(N_c)$ theories is hindered by the divergence of the integrated autocorrelation time $\tau_Q N_{sw}$, as $a \to 0$ [59]. This phenomenon, known as *topological freezing*, descends from the intrinsic difficulty of evolving with a local update algorithm a global property such as the topological charge. We expect the same challenge to arise in $Sp(2N)$ theories. Several ideas have been put forward to overcome topological freezing [68–70,84–86], but we defer their use to future high precision studies. Here, we limit ourselves to monitoring the values of τ_Q, and discarding compromised ensembles.

III. SCALE SETTING AND TOPOLOGY

The definition of the continuum limit requires the implementation of a scale-setting procedure. A scale is introduced by selecting a dimensional quantity that can (in principle) be measured both in the physical limit and on the lattice. All physical quantities $\langle \mathcal{O} \rangle$ are expressed in terms of such scale, and measurements are repeated by varying the lattice parameters (in the present case, β). The extrapolation towards $a \to 0$ yields then a finite value of $\langle \mathcal{O} \rangle$, in the chosen units.

The string tension, σ, of Yang-Mills theories is defined as the coefficient of the linear term of the potential between an infinitely massive, *static* pair of fermion and antifermion transforming in the fundamental representation, in the regime of asymptotically large separation. On the lattice, it can be extracted from the asymptotic behavior of appropriately defined 2-points correlators in Euclidean time. Thanks to its direct physical interpretation, σ is often used for scale setting in studies of the properties of the confining phase of pure gauge theories—see, e.g., Refs. [46,55,59,66,68,75]. However, it suffers from the effect of both systematic and statistical errors that limit the precision of its measurement. Most importantly, the definition of σ is problematic in the presence of string breaking effects, which would emerge in the presence of matter fields. In this paper we adopt an alternative strategy, which could be adapted to more general gauge theories with fermionic matter field content. We will return to using σ to set the scale for the topological susceptibility in Ref. [75], as it will help in the comparison with measurements of χ in $SU(N_c)$ Yang-Mills theories.

The gradient flow $B_\mu(x,t)$ [76,77] is defined unambiguously in the continuum as on the lattice, with or without matter fields, and it can be determined precisely from simple averages of lattice observables. It is introduced as the solution to the differential equation

$$\frac{\mathrm{d}B_\mu(x,t)}{\mathrm{d}t} = D_\nu G_{\nu\mu}(x,t), \tag{20}$$

with boundary conditions $B_\mu(x,0) = A_\mu(x)$. The independent variable t is known as *flow time*, while $D_\mu \equiv \partial_\mu + [B_\mu, \cdot]$, with

$$G_{\mu\nu}(t) = [D_\mu, D_\nu]. \tag{21}$$

The defining properties of the gradient flow make it suitable as a smoothening procedure for UV fluctuations. Since $\frac{d}{dt} S_{\mathrm{YM}} \leq 0$, a representative configuration $A_\mu(x)$ at $t = 0$ is driven, along the flow, towards a classical configuration. In the perturbative regime, the flow equation can be shown, at leading order in g_0, to generate a Gaussian smoothening operation with mean-square radius $\sqrt{8t}$. As a consequence, short-distance singularities in correlation functions of operators at $t > 0$ are eliminated.

The renormalized coupling α at scale $\mu = 1/\sqrt{8t}$ is

$$\alpha(\mu) \equiv k_\alpha t^2 \langle E(t) \rangle \equiv k_\alpha \mathcal{E}(t), \tag{22}$$

where k_α is a (perturbatively) calculable constant, and

$$E(t) \equiv \frac{1}{2} \mathrm{Tr} G_{\mu\nu}(t) G_{\mu\nu}(t). \tag{23}$$

The evolution of $\alpha(1/\sqrt{8t})$ defines implicitly the scale $1/\sqrt{8t_0}$ of the system, by the requirement

$$\mathcal{E}(t)|_{t=t_0} = \mathcal{E}_0, \tag{24}$$

where $\mathcal{E}_0$ is a reference value, chosen for convenience.

Alternatively, one defines the observable [87]

$$\mathcal{W}(t) \equiv t \frac{d}{dt} \{ t^2 \langle \mathcal{E}(t) \rangle \}, \tag{25}$$

and the scale w_0 is defined implicitly from

$$\mathcal{W}(t)|_{t=w_0^2} = \mathcal{W}_0, \tag{26}$$

where again $\mathcal{W}_0$ is a reference constant value. While $\mathcal{E}(t)$ is expected to be sensitive to the fluctuations of the gauge configurations on scales *down to* $1/\sqrt{t_0}$, $\mathcal{W}(t)$ only depends on fluctuations *around* $1/\sqrt{t_0}$.

We will compute the value of t_0 and w_0 in $Sp(N_c)$ theories for different values of N_c, with the implicit intention of exploring the $N_c \to \infty$ limit at constant 't Hooft coupling $\lambda \equiv 4\pi N_c \alpha$. From the perturbative relation between $\mathcal{E}(t)$ and the gradient flow coupling [76], we obtain the leading-order expression

$$\mathcal{E}(t) = \frac{3\lambda}{64\pi^2} C_2(F), \tag{27}$$

with $C_2(F) = \frac{N_c+1}{4}$, the quadratic Casimir operator of the fundamental representation of $Sp(N_c)$. In order to compare

different $Sp(N_c)$ theories, we scale $\mathcal{E}_0$ and $\mathcal{W}_0$ according to the following relations:

$$\mathcal{E}_0(N_c) = c_e C_2(F), \qquad \mathcal{W}_0(N_c) = c_w C_2(F), \tag{28}$$

where c_e and c_w are constants. From Eq. (27), leading-order perturbation theory gives

$$c_e = \frac{3\lambda}{64\pi^2}, \tag{29}$$

showing that c_e determines the fixed-λ trajectory along which to take the $N_c \to \infty$ limit.[1] Whether the scaling law in Eq. (28) holds outside of the domain of validity of perturbation theory is a question we return to in Sec. IV.

A. The Wilson flow

The lattice incarnation of the gradient flow is based on the Wilson action S_W in Eq. (11), and is known as the Wilson flow. $V_\mu(x,t)$ is defined by solving

$$\frac{\partial V_\mu(x,t)}{\partial t} = -g_0^2\{\partial_{x,\mu} S^{\text{flow}}[V_\mu]\}V_\mu(x,t), \tag{30}$$

where $V_\mu(x,0) = U_\mu(x)$. The properties of the Wilson flow are naturally inherited from the continuum formulation. Moreover, a numerical integration can be set up to obtain $V_\mu(x,t)$ from $U_\mu(x)$ explicitly, using for example a Runge-Kutta integration scheme, as detailed in Ref. [76]. Observables can then be constructed from $V_\mu(x,t)$.

To use the Wilson flow as a scale-setting procedure requires the computation of $\mathcal{E}(t)$ or $\mathcal{W}(t)$, for which purpose two alternative lattice discretizations of $G_{\mu\nu}(t)$ can be used. One is the elementary plaquette operator defined in Eq. (10), computed from $V_\mu(t)$. The other is the four-plaquette clover leaf in Eq. (13). By comparing numerically the values of $\mathcal{E}(t)$ and $\mathcal{W}(t)$, as well as the two different discretizations, we can assess the magnitude of discretization errors in approaching the continuum limit.

B. Topological susceptibility on the lattice

As anticipated in Sec. II, we compute the topological susceptibility on the lattice from Wilson-flowed configurations. At flow time t, the topological charge density can be obtained from

$$q_L(t,x) \equiv \frac{1}{32\pi^2}\epsilon^{\mu\nu\rho\sigma}\text{Tr}\mathcal{C}_{\mu\nu}(x,t)\mathcal{C}_{\rho\sigma}(x,t), \tag{31}$$

where $\mathcal{C}_{\mu\nu}(x,t)$ is the clover operator computed from $V_\mu(x,t)$. The topological charge is $Q_L(t) = \sum_x q_L(x,t)$.

[1]For unitary groups $SU(N_c)$, $C_2(F) = (N_c^2-1)/(2N_c)$. The choice $c_e = 9/40$ would yield $\mathcal{E}_0 = 0.3$ for $SU(3)$ [76].

On the lattice, the values of the topological charge are quasi-integers, affecting the measurement of χ_L. Following Ref. [66], we reduce this systematical error by redefining $\tilde{Q}_L$ as follows:

$$\tilde{Q}_L(t) \equiv \text{round}\Big(\tilde{\alpha}\sum_x q_L(x,t)\Big), \tag{32}$$

where $\tilde{\alpha}$ is a numerical factor determined by minimizing the t-dependent quantity

$$\Delta(\tilde{\alpha}) = \langle[\tilde{\alpha}Q_L - \text{round}(\tilde{\alpha}Q_L)]^2\rangle. \tag{33}$$

We will provide an illustrative example of the choice of numerical factor $\tilde{\alpha} \sim \mathcal{O}(1)$ when presenting our results. The topological susceptibility at flow time t is then

$$\chi_L(t)a^4 = \frac{1}{L^4}\langle\tilde{Q}_L(t)^2\rangle. \tag{34}$$

IV. NUMERICAL RESULTS

We generated and stored ensembles of thermalized configurations for the set of bare parameters listed in the three leftmost columns of Table I. From a comparison with the results obtained for σ in Ref. [15], we know that $\sqrt{\sigma}L \geq 3$ for all such ensembles, and neglect finite-volume effects. In the following, we present and discuss our

TABLE I. Ensembles used for scale setting. The first three columns show the bare parameters for each ensemble. N_{tot} is the number of configurations, and we applied N_{sw} lattice sweeps between two successive configurations. The measurement of the integrated autocorrelation time of the topological charge, τ_Q, is discussed later in the paper.

N_c	L/a	β	N_{sw}	N_{tot}	τ_Q
2	20	2.55	50	3999	0.512(30)
2	24	2.60	100	3999	0.512(30)
2	32	2.65	100	4003	0.561(33)
2	32	2.70	100	4003	0.729(43)
4	20	7.7	50	4000	0.644(38)
4	20	7.72	50	4000	0.672(40)
4	20	7.76	50	4000	0.779(52)
4	20	7.78	40	4002	1.079(80)
4	20	7.80	80	4021	0.691(41)
4	20	7.85	70	4002	1.104(82)
4	24	8.2	3500	3898	0.550(33)
6	18	15.75	60	4000	0.848(57)
6	16	15.9	100	4006	0.959(64)
6	16	16.1	400	4011	1.170(87)
6	20	16.3	800	4001	1.47(12)
8	16	26.5	600	3924	0.617(37)
8	16	26.7	400	4061	1.27(10)
8	16	27.0	1200	3887	1.50(13)
8	16	27.2	3000	4107	1.245(99)

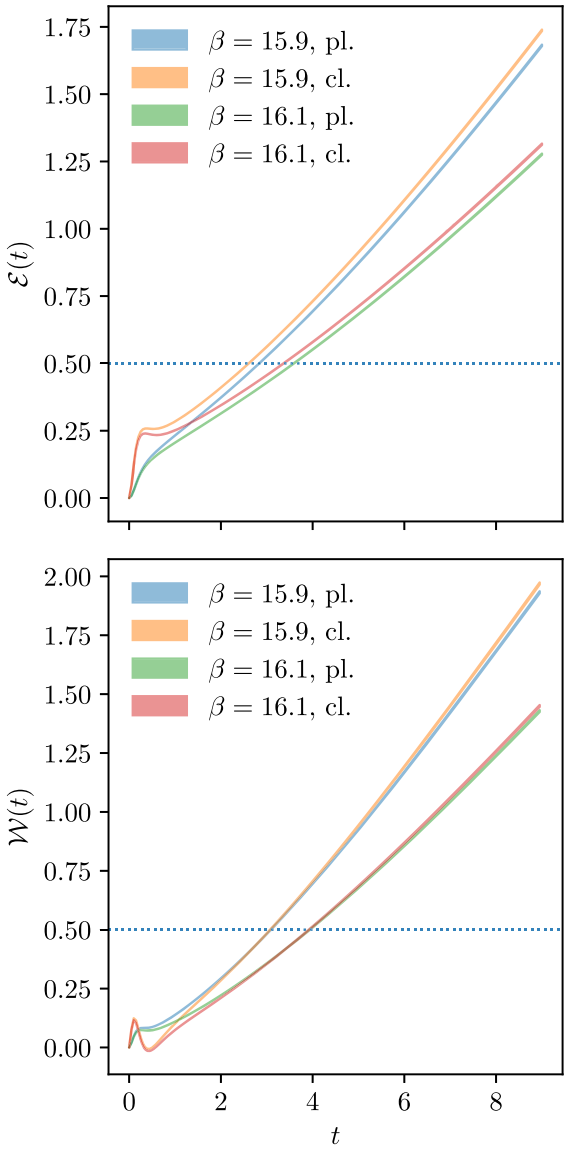

FIG. 1. The quantities $\mathcal{E}(t)$ (top panel) and $\mathcal{W}(t)$ (bottom panel), defined in Eqs. (22) and (23), and in Eq. (25), respectively, in the $N_c = 6$ ensembles with $\beta = 15.9$ and $\beta = 16.3$, as functions of the flow time t. Computations adopt the alternative choices of discretization provided by the elementary plaquette (pl.) and the clover-leaf plaquette (cl.). The horizontal dashed line represents the choice $\mathcal{E}_0 = 0.5$, $\mathcal{W}_0 = 0.5$.

numerical results for the scale-setting procedure, and for the topological susceptibility.

A. Setting the scale

Each configuration in the ensembles in Table I sets the initial conditions for the numerical integration of the Wilson flow, which obeys Eq. (30). Following Ref. [76], we use a third-order Runge-Kutta integrator (implemented by HiRep [80]) to evaluate $V_\mu(x,t)$ in the range $0 < t < t_{\text{max}}$, with t_{max} such that $\sqrt{8t_{\text{max}}} \lesssim L/2$, to avoid large finite size effects.

TABLE II. The gradient flow scale $\sqrt{t_0}/a$ for different choices of β and $\mathcal{E}_0$, for $N_c = 6$. We report the results for both the plaquette and clover discretizations.

β	$\mathcal{E}_0$	$\sqrt{t_0}/a$ (pl.)	$\sqrt{t_0}/a$ (cl.)
15.75	0.3	0.92442(25)	1.11491(20)
15.9	0.3	1.07199(36)	1.22045(33)
16.1	0.3	1.24921(48)	1.36866(47)
16.3	0.3	1.42716(42)	1.52798(41)
15.75	0.4	1.24407(31)	1.34614(29)
15.9	0.4	1.38876(49)	1.47758(49)
16.1	0.4	1.58507(71)	1.66099(69)
16.3	0.4	1.79128(63)	1.85737(60)
15.75	0.5	1.45355(39)	1.53196(37)
15.9	0.5	1.61449(63)	1.68380(63)
16.1	0.5	1.83487(92)	1.89487(89)
16.3	0.5	2.06770(82)	2.12034(78)
15.75	0.6	1.62169(46)	1.68890(44)
15.9	0.6	1.79810(76)	1.85783(76)
16.1	0.6	2.0401(11)	2.0920(11)
16.3	0.6	2.2960(10)	2.34178(95)

The quantity $\mathcal{E}(t)$ is obtained from the definitions in Eqs. (22) and (23), by computing $G_{\mu\nu}$ from B_μ. We use two alternative discretized expressions for $\mathcal{E}(t)$, provided by the plaquette (pl.), $\mathcal{P}_{\mu\nu}$, or the clover leaf (cl.), $\mathcal{C}_{\mu\nu}$. We then compute $\mathcal{W}(t)$ according to Eq. (25). The resampled results for $\mathcal{E}(t)$ and $\mathcal{W}(t)$, as functions of t, are displayed in the two panels of Fig. 1, in the case $N_c = 6$, with $\beta = 15.9$ and $\beta = 16.3$ and for the two different discretizations (pl. and cl.). For each value of t, the vertical thickness of the curves

TABLE III. The gradient flow scale w_0/a for different choices of β and $\mathcal{W}_0$, for $N_c = 6$. We report the results for both the plaquette and clover discretizations.

β	$\mathcal{W}_0$	w_0/a (pl.)	w_0/a (cl.)
15.75	0.3	1.14525(18)	1.13768(17)
15.9	0.3	1.20091(29)	1.19500(29)
16.1	0.3	1.27407(40)	1.26968(38)
16.3	0.3	1.34793(34)	1.34454(32)
15.75	0.4	1.20835(21)	1.20698(20)
15.9	0.4	1.26876(33)	1.26784(33)
16.1	0.4	1.34754(46)	1.34701(44)
16.3	0.4	1.42652(39)	1.42624(37)
15.75	0.5	1.26030(23)	1.26195(22)
15.9	0.5	1.32419(37)	1.32572(37)
16.1	0.5	1.40712(51)	1.40852(48)
16.3	0.5	1.48995(43)	1.49123(41)
15.75	0.6	1.30458(25)	1.30797(24)
15.9	0.6	1.37126(40)	1.37421(40)
16.1	0.6	1.45758(55)	1.46009(53)
16.3	0.6	1.54353(47)	1.54572(45)

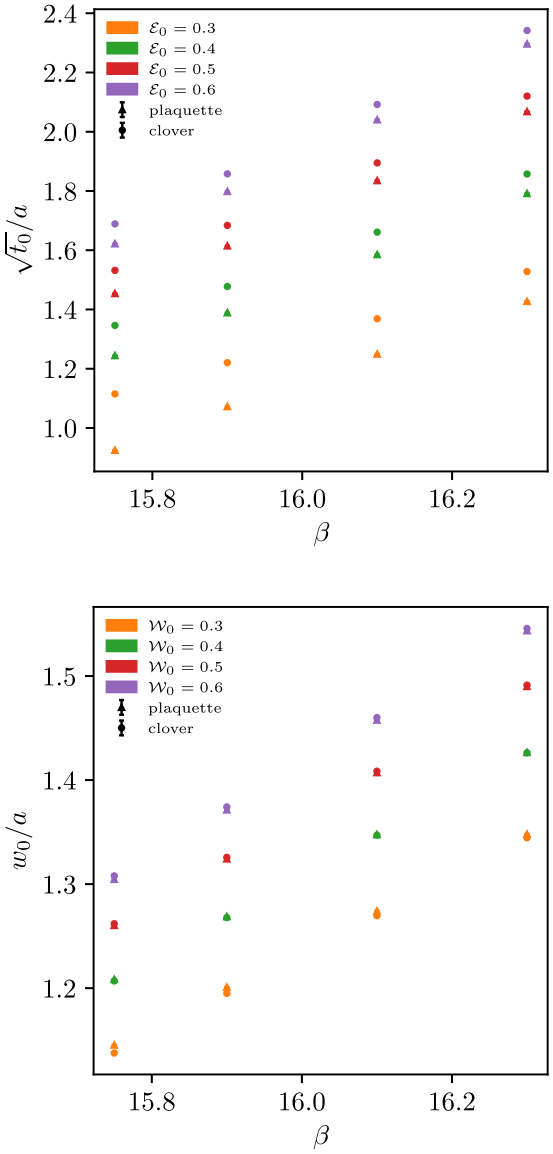

FIG. 2. The gradient flow scales $\sqrt{t_0}/a$ (top panel) and w_0/a (bottom) in $Sp(6)$, for different choices of $\mathcal{E}_0$ or $\mathcal{W}_0$, as a function of β, and comparing plaquette and clover discretization. In the case of w_0/a, the difference between discretizations is barely discernible over the statistical uncertainty.

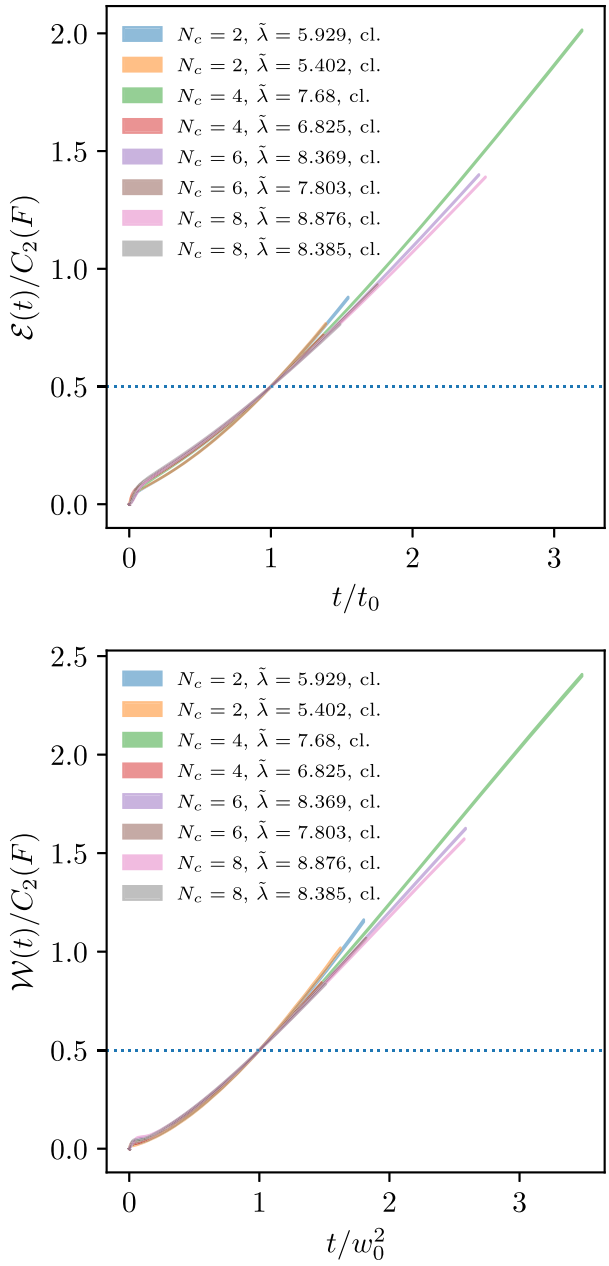

FIG. 3. The quantities $\mathcal{E}(t)/C_2(F)$ (top panel) and $\mathcal{W}(t)/C_2(F)$ (bottom) computed with the clover-leaf plaquette discretization of the flow equation on the available ensembles corresponding to the finest and coarsest available lattices, for each N_c, with $C_2(F) = (N_c + 1)/4$, displayed as a function of the rescaled flow times t/t_0 and t/w_0^2. The figure adopts the choice $c_e = c_w = 0.5$ (horizontal dashed line).

represents the error of $\mathcal{E}(t)$ and $\mathcal{W}(t)$, computed by bootstrapping. The picture is qualitatively the same for other values of the bare parameters and is similar to the $SU(N_c)$ case.

From $\mathcal{E}(t)$ and $\mathcal{W}(t)$ we can extract the scales t_0 and w_0, according to the definitions in Eqs. (24) and (26), once we make a choice for the reference values $\mathcal{E}_0$ and $\mathcal{W}_0$. For illustrative purposes, the choices $\mathcal{E}_0 = 0.5$ and $\mathcal{W}_0 = 0.5$ are represented as horizontal dashed lines in the top and bottom panel of Fig. 1, though we do not use this choice in the analysis. The comparison between $\mathcal{E}(t)$ and $\mathcal{W}(t)$ provides a first assessment of the magnitude of discretization effects in the calculation. For each ensemble, the difference between the curves corresponding to the plaquette and clover discretizations tends to a constant at large t. This difference is the smallest in the ensemble with the largest value of β—the closest to the continuum limit—and is smaller for $\mathcal{W}(t)$ than $\mathcal{E}(t)$, as anticipated in Sec. III.

A more refined assessment of discretization effects can be obtained by studying the value of the scales $\sqrt{t_0}/a$ and w_0/a, obtained for a range of choices of $\mathcal{E}_0$ and $\mathcal{W}_0$, for each

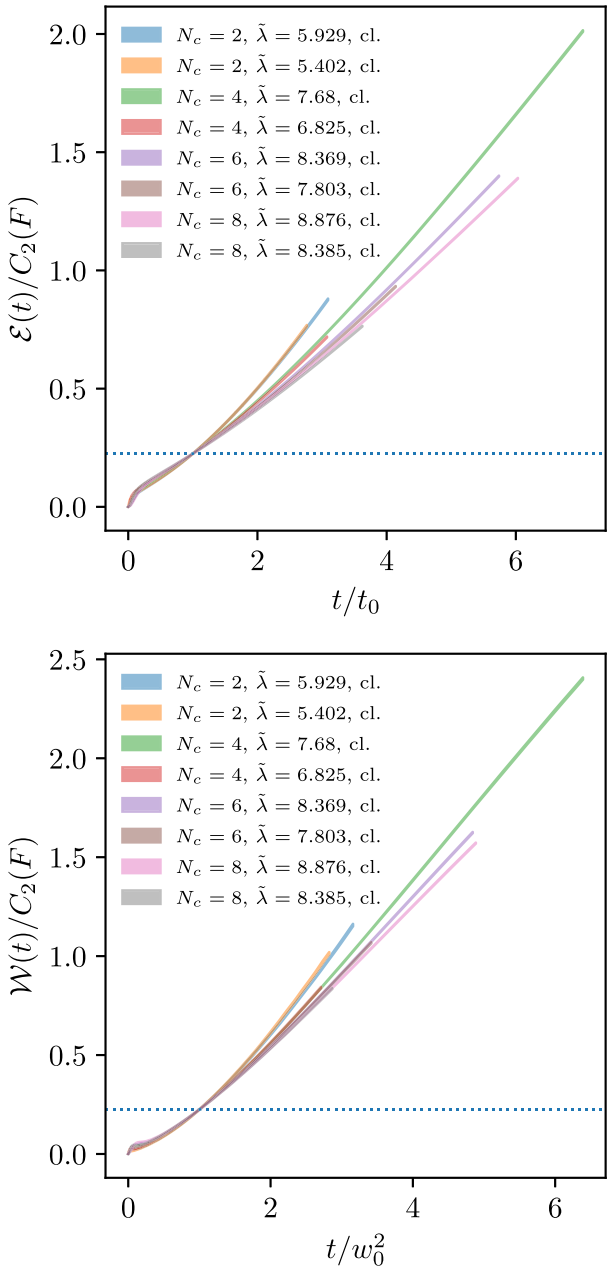

FIG. 4. The quantities $\mathcal{E}(t)/C_2(F)$ (top panel) and $\mathcal{W}(t)/C_2(F)$ (bottom) computed with the clover-leaf plaquette discretization of the flow equation on the available ensembles corresponding to the finest and coarsest lattices, for each N_c, with $C_2(F) = (N_c + 1)/4$, displayed as a function of the rescaled flow times t/t_0 and t/w_0^2. The figure adopts the choice $c_e = c_w = 0.225$ (horizontal dashed line).

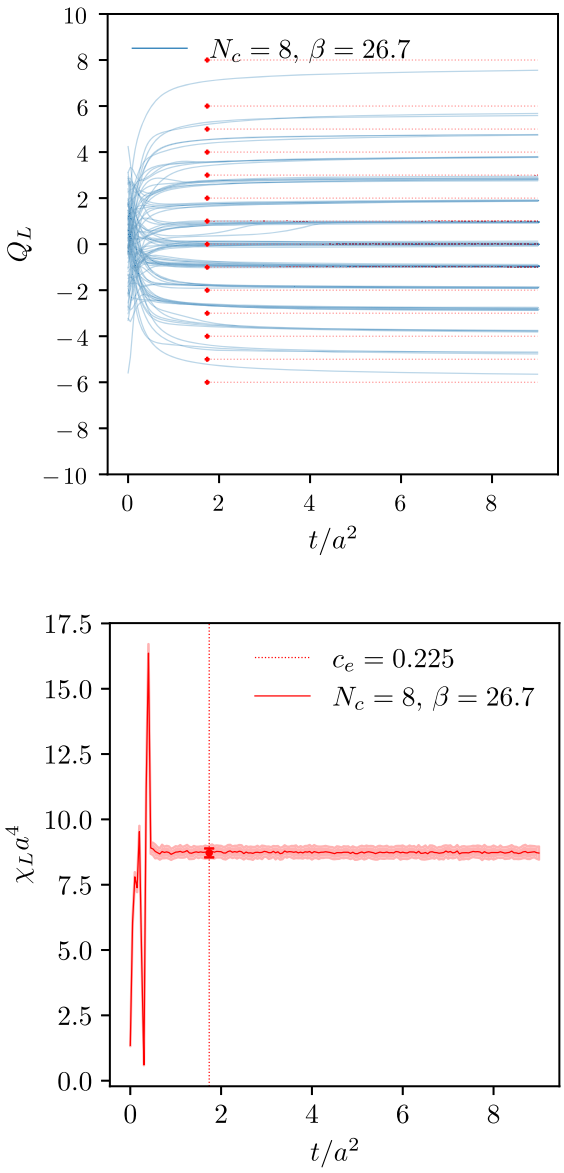

FIG. 5. In the top panel, he topological charge Q_L as a function of the flow time t/a^2, for the 100 first configurations of the ensemble with $N_c = 8$, $L/a = 16$, and $\beta = 26.7$. The values of $\tilde{Q}_L$ are also reported as red bullets at $t = t_0$, where t_0 is obtained from the choice $c_e = 0.225$. In the bottom panel, the topological susceptibility $\chi_L(t)a^4$ as a function of the flow time t, with its 1-σ error band, for $N_c = 8$, at $\beta = 26.7$. The vertical dashed represents $t = t_0$, where t_0 is obtained from $c_e = c_w = 0.225$. The value of $\chi_L(t = t_0)a^4$ obtained at $t = t_0$ is depicted as a red bullet and reported in Table IV.

available ensemble, which we report in Tables II and III, and display in Fig. 2 for $Sp(6)$. The difference between the plaquette and clover discretizations becomes smaller as β is increased. This difference has generally a smaller magnitude for the w_0 scale than for $\sqrt{t_0}$ scale. A similar picture emerges for $N_c = 2$, $N_c = 4$, and $N_c = 8$. as reported in the Appendix. In view of these considerations, we adopt the clover discretization in the following.

In Sec. III, we observed that the functions $\mathcal{E}(t)$ and $\mathcal{W}(t)$ obey perturbative relations that suggest the scaling behavior in Eq. (28). The numerical data we have collected allows to test the validity of these scaling relations outside of the domain of perturbation theory. We choose values of $\mathcal{E}_0$ and $\mathcal{W}_0$ for each value of N_c according to Eq. (28), with fixed c_e and c_w. The corresponding values of t_0 and w_0 are then used to scale also t.

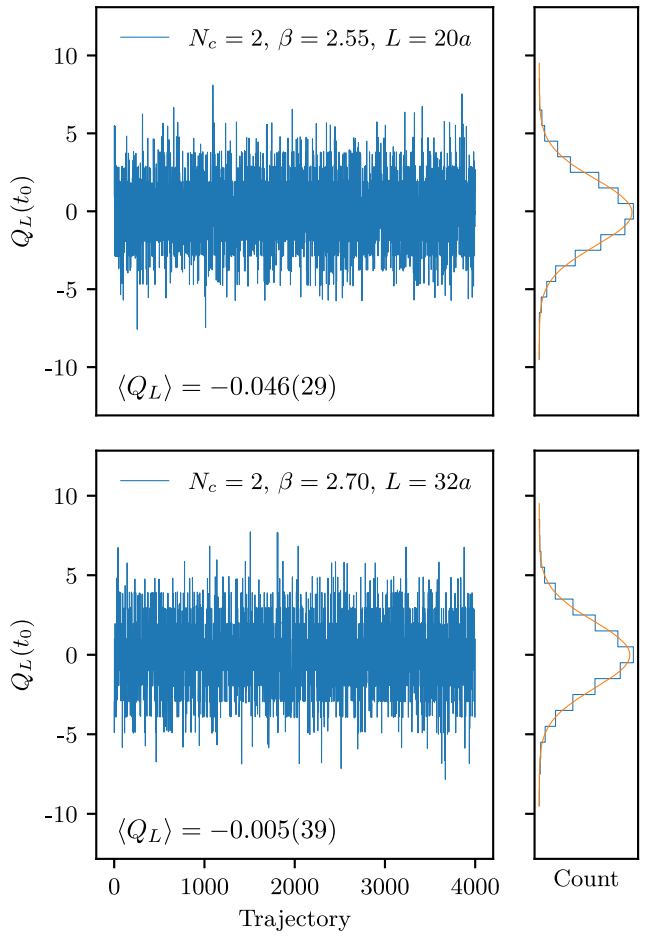

FIG. 6. The topological charge Q_L as a function of simulation time (trajectory) for the ensembles corresponding to the coarsest (top) and finest (bottom) lattice with $N_c = 2$. The value of Q_L is computed at $t = t_0$, where the value of t_0 is obtained from $c_e = 0.225$. The average value of the topological charge along the trajectory is reported in the bottom left-hand side of plot. The side panel contains the cumulative histogram of the values of $Q_L(t_0)$. The orange curve is a Gaussian fit to the cumulative histogram.

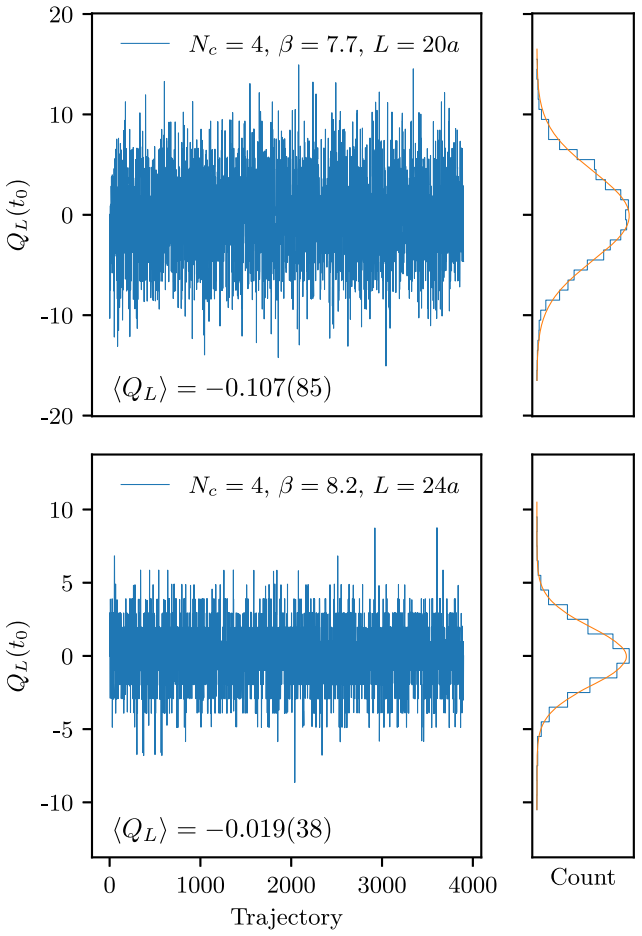

FIG. 7. The topological charge Q_L as a function of simulation time (trajectory) for the ensembles corresponding to the coarsest (top) and finest (bottom) lattice with $N_c = 4$. The value of Q_L is computed at $t = t_0$, where the value of t_0 is obtained from $c_e = 0.225$. The average value of the topological charge along the trajectory is reported in the bottom left-hand side of plot. The side panel contains the cumulative histogram of the values of $Q_L(t_0)$. The orange curve is a Gaussian fit to the cumulative histogram.

The result of these operations, with the clover-leaf discretization, and at each fixed value of N_c, for the ensembles with the smallest and the greatest values of β, are displayed in Fig. 3 for the choice $c_e = c_w = 0.5$. The plots exhibit the same qualitative features for both $\mathcal{E}(t)/C_2(F)$ and $\mathcal{W}(t)/C_2(F)$ as functions of t/t_0 and t/w_0^2, respectively. We repeat the same process also for the choice $c_e = c_w = 0.225$ [which would yield $\mathcal{E}_0 = 0.3$ for $SU(3)$], and display the results in Fig. 4. We labeled the curves by the conveniently defined discretized coupling

$$\tilde{\lambda} \equiv \frac{d_G}{\beta \langle \frac{\Re \mathrm{Tr} \mathcal{P}_{\mu\nu}}{2N} \rangle}, \tag{35}$$

where d_G is the dimension of the group.

By construction, the rescaled flows corresponding to different values of N_c coincide when $t/t_0 = 1$ (or $t/w_0^2 = 1$). What is interesting is that the curves agree (within uncertainties) over a sizeable range of t around these points. This might indicate that the validity of the perturbative scaling in Eq. (28) holds also outside of the naive range of the perturbative regime. Small deviations from perfect scaling are nevertheless visible and might be ascribed to a combination of finite-a and finite-N_c effects.

B. The topological charge

The quantity $Q_L(t)$ is computed from Wilson-flowed configurations at flow time t, using Eq. (31), as implemented by HiRep [80]. Figure 5 is compiled with the first 100 configurations of the ensemble with $N_c = 8$ and $\beta = 26.7$. Integer values for $Q_L(t)$ are only obtained for $a \to 0$. At nonzero a, the quantity $Q_L(t)$ tends, at large t, towards quasi-integer values. The integer-valued topological charge $\tilde{Q}_L$ is instead obtained for a finite value of t,

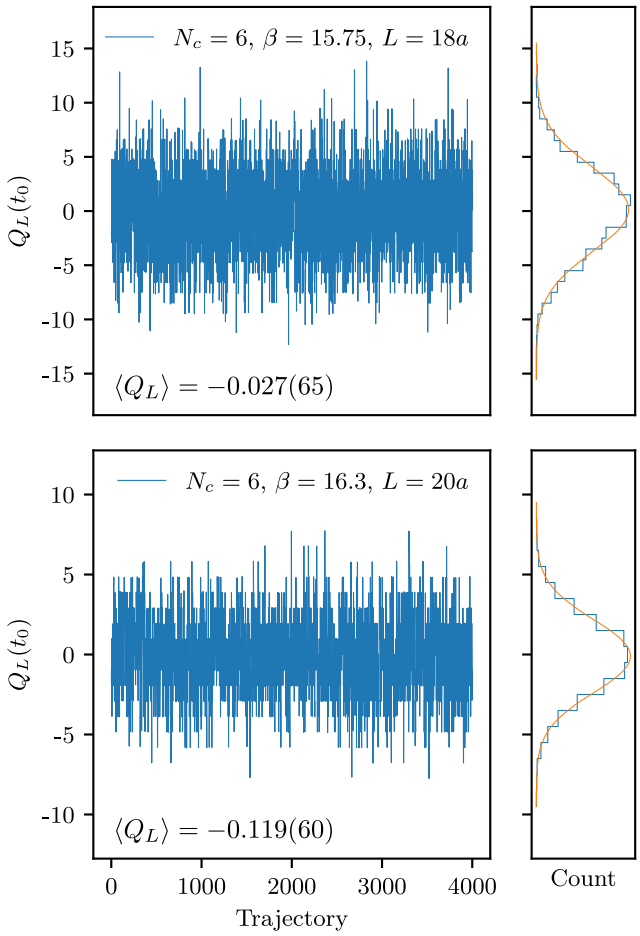

FIG. 8. The topological charge Q_L as a function of simulation time (trajectory) for the ensembles corresponding to the coarsest (top) and finest (bottom) lattice with $N_c = 6$. The value of Q_L is computed at $t = t_0$, where the value of t_0 is obtained from $c_e = 0.225$. The average value of the topological charge along the trajectory is reported in the bottom left-hand side of plot. The side panel contains the cumulative histogram of the value. The orange curve is a Gaussian fit to the cumulative histogram. es of $Q_L(t_0)$.

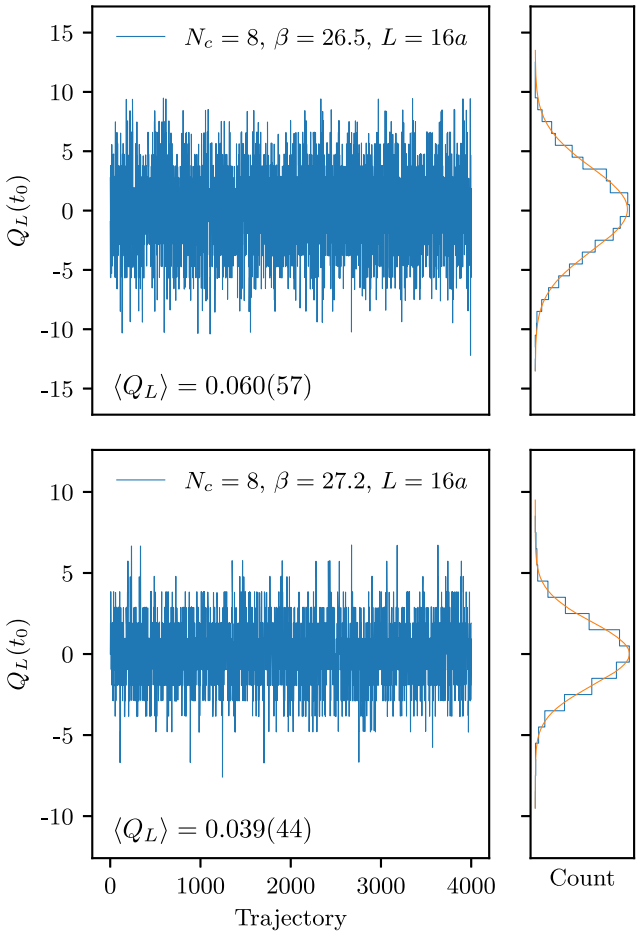

FIG. 9. The topological charge Q_L as a function of simulation time (trajectory) for the ensembles corresponding to the coarsest (top) and finest (bottom) lattice with $N_c = 8$. The value of Q_L is computed at $t = t_0$, where the value of t_0 is obtained from $c_e = 0.225$. The average value of the topological charge along the trajectory is reported in the bottom left-hand side of plot. The side panel contains the cumulative histogram of the values of $Q_L(t_0)$. The orange curve is a Gaussian fit to the cumulative histogram.

according to Eq. (32). The values of $\tilde{Q}_L$ are displayed in Fig. 5 as red bullets, and for the value of $t = t_0$ identified with the choice $c_e = 0.225$. Effectively this definition of $\tilde{Q}_L$ optimizes and expedites the convergence towards the physical, discrete values of the topological charge. Similar conclusions hold for other values of the bare parameters, though we do not report further details here. In the following, we will compute $\tilde{Q}_L$ for every configuration of every ensemble at both $c_e = 0.225$ and $c_e = 0.5$.

Simulation histories of Q_L for the ensembles with the finest and coarsest lattice are displayed in Figs. 6, 7, 8, and 9, for $N_c = 2$, 4, 6, 8, respectively. The frequency histogram for the values of Q_L is also reported, in each case, and is consistent with a Gaussian, symmetric distribution around $Q_L = 0$.

The magnitude of autocorrelations can be evaluated using the Madras-Sokal windowing algorithm [90] on the simulation history of either Q_L or $\tilde{Q}_L$. For our ensembles, we found no significant difference to arise between the two, and no visible dependence on the choice of c_e. We thus compute τ_Q at $t = t_0$, for $c_e = 0.225$. The behavior of the logarithm of $\tau_Q N_{\mathrm{sw}}$ as a function of β is displayed in Fig. 10 and reported in Table I. On the basis of known results obtained for $SU(N_c)$ gauge groups, $\ln \tau_Q N_{\mathrm{sw}}$ is expected to be linearly diverging as $\beta \to \infty$ [59], and indeed this is consistent with what we find.

The topological susceptibility in lattice units $\chi_L(t)a^4$ was computed for each ensemble separately, using Eq. (34). The effect of the rounding procedure, Eq. (32), on the topological susceptibility, is displayed in Fig. 5, where $\chi_L(t)a^4$ is plotted as a function of the flow time t/a^2. For sufficiently large values of the flow time, $\chi_L(t)a^4$ is compatible with a constant within errors. The value of $\chi_L t_0^2$ computed at the scale t_0, obtained from $c_e = w_e = 0.225$,

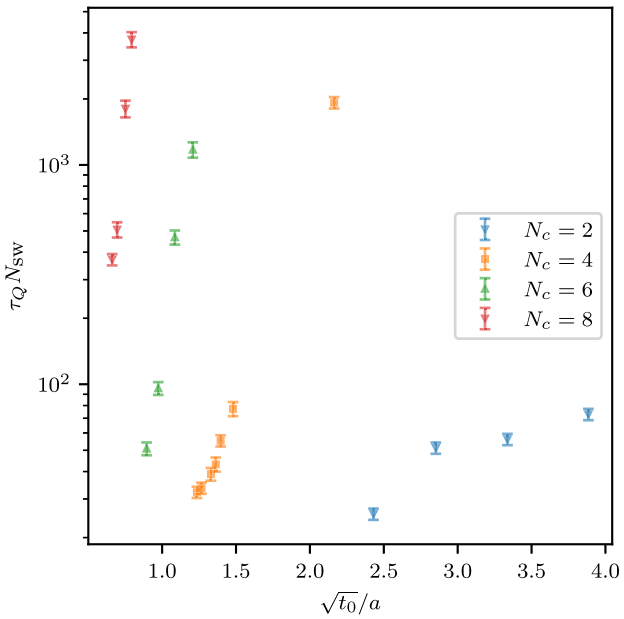

FIG. 10. The integrated autocorrelation time τ_Q multiplied by the number of sweeps $N_{\rm sw}$, as a function of the scale $\sqrt{t_0}/a$, for $c_e = 0.225$ for $N_c = 2, 4, 6, 8$.

is displayed as a red bullet. We report the results for the choices $c_e = c_w = 0.225$ and $c_e = c_w = 0.5$, in Tables IV and V, respectively. For convenience, we also report the values of σt_0 and σw_0^2, which are taken from Ref. [15],

TABLE IV. Topological susceptibilities $\chi_L t_0^2$ and $\chi_L w_0^4$, with $c_e = c_w = 0.225$, and the string tensions σt_0 and σw_0^2, for all available ensembles. These results are displayed as a function of a^2/t_0 and a^2/w_0^2 in Fig. 11.

N_c	β	σt_0	$\chi_L t_0^2 \times 10^4$	σw_0^2	$\chi_L w_0^4 \times 10^4$
2	2.55	0.11440(93)	6.69(16)	0.11164(92)	6.40(15)
2	2.6	0.1120(11)	6.39(12)	0.1090(10)	6.07(14)
2	2.65	0.1120(20)	6.55(14)	0.1092(19)	6.21(14)
2	2.7	0.1097(18)	6.17(14)	0.1070(18)	5.87(17)
4	7.7	0.1029(24)	5.19(12)	0.1127(26)	6.47(15)
4	7.72	0.1035(28)	5.52(12)	0.1138(31)	6.80(16)
4	7.76	0.0987(29)	5.50(11)	0.1087(32)	6.71(16)
4	7.78	0.1028(29)	5.29(15)	0.1136(32)	6.44(15)
4	7.8	0.0988(23)	5.06(12)	0.1093(26)	6.16(15)
4	7.85	0.1013(14)	5.18(13)	0.1125(16)	6.40(16)
4	8.2	0.1036(16)	4.79(12)	0.1171(18)	6.11(15)
6	15.75	0.0972(12)	4.61(12)	0.1146(15)	6.36(15)
6	15.9	0.0988(13)	4.244(93)	0.1177(15)	5.98(13)
6	16.1	0.0947(16)	4.19(10)	0.1138(20)	6.06(15)
6	16.3	0.0955(33)	3.85(10)	0.1153(40)	5.61(15)
8	26.5	0.0953(13)	4.146(78)	0.1170(16)	6.27(11)
8	26.7	0.0954(26)	4.03(11)	0.1181(32)	6.16(17)
8	27.0	0.0942(14)	3.99(10)	0.1177(17)	6.23(18)
8	27.2	0.0905(13)	3.606(90)	0.1138(17)	5.72(18)

TABLE V. Topological susceptibilities $\chi_L t_0^2$ and $\chi_L w_0^4$, with $c_e = c_w = 0.5$, and the string tensions σt_0 and σw_0^2, for all available ensembles. These results are displayed as a function of a^2/t_0 and a^2/w_0^2 in Fig. 11.

N_c	β	σt_0	$\chi_L t_0^2 \times 10^3$	σw_0^2	$\chi_L w_0^4 \times 10^3$
2	2.55	0.2289(19)	2.547(58)	0.1956(16)	1.881(47)
2	2.6	0.2235(21)	2.448(49)	0.1907(18)	1.789(35)
2	2.65	0.2233(39)	2.527(60)	0.1902(33)	1.840(40)
2	2.7	0.2186(37)	2.388(63)	0.1861(31)	1.736(45)
4	7.7	0.2265(52)	2.510(60)	0.2070(47)	2.100(51)
4	7.72	0.2281(62)	2.669(76)	0.2087(56)	2.246(56)
4	7.76	0.2178(63)	2.647(59)	0.1992(58)	2.225(46)
4	7.78	0.2271(64)	2.556(61)	0.2080(59)	2.137(57)
4	7.8	0.2186(51)	2.430(53)	0.2001(47)	2.040(48)
4	7.85	0.2246(31)	2.507(67)	0.2060(29)	2.113(53)
4	8.2	0.2323(36)	2.399(62)	0.2146(33)	2.055(47)
6	15.75	0.2261(29)	2.468(49)	0.2147(28)	2.221(50)
6	15.9	0.2313(30)	2.317(53)	0.2208(29)	2.103(47)
6	16.1	0.2230(38)	2.310(56)	0.2136(37)	2.126(53)
6	16.3	0.2254(78)	2.137(56)	0.2162(75)	1.975(60)
8	26.5	0.2285(31)	2.380(49)	0.2220(30)	2.248(45)
8	26.7	0.2301(63)	2.345(70)	0.2243(61)	2.230(65)
8	27.0	0.2285(33)	2.351(76)	0.2236(32)	2.244(66)
8	27.2	0.2204(32)	2.149(64)	0.2161(32)	2.057(51)

except for $\beta = 2.55, 2.65$ for $N_c = 2$, and $\beta = 7.72, 7.76, 7.78$ and 7.80 for $N_c = 4$, which we computed anew.

Our final results are the extrapolations towards the continuum limit of $\chi_L t_0^2$ for each of the $Sp(N_c)$ Yang-Mills theories. We obtain these by assuming the following functional dependence:

TABLE VI. Continuum limit extrapolations obtained from the best fit of Eq. (36) for the topological susceptibility in $Sp(N_c)$ Yang-Mills theories with $N_c = 2, 4, 6, 8$. We present four alternative ways of setting the scale: we measure $\chi t_0^2(a = 0)$ (top section of the table) and $\chi w_0^4(a = 0)$ (bottom), and adopt as reference values either $c_e = 0.225 = c_w$ (left section of the table) or $c_e = 0.5 = c_w$ (right). The best-fit curves are displayed as dashed lines in Fig. 11, for each value of N_c, along with the individual measurements.

N_c	$\chi_L t_0^2(a=0)$	$\tilde{\chi}^2$	$\chi_L t_0^2(a=0)$	$\tilde{\chi}^2$
	$c_e = 0.225$		$c_e = 0.5$	
2	0.000600(22)	1.47	0.002353(93)	1.29
4	0.000452(17)	2.18	0.002305(90)	1.89
6	0.000315(23)	1.08	0.00185(11)	1.02
8	0.000303(23)	2.32	0.00194(15)	1.39
N_c	$\chi_L w_0^4(a=0)$ $c_w = 0.225$	$\tilde{\chi}^2$	$\chi_L w_0^4(a=0)$ $c_w = 0.5$	$\tilde{\chi}^2$
2	0.000572(24)	1.16	0.001698(69)	1.50
4	0.000584(22)	1.63	0.001991(69)	2.14
6	0.000503(32)	1.39	0.00180(12)	1.13
8	0.000535(39)	1.41	0.00189(13)	1.80

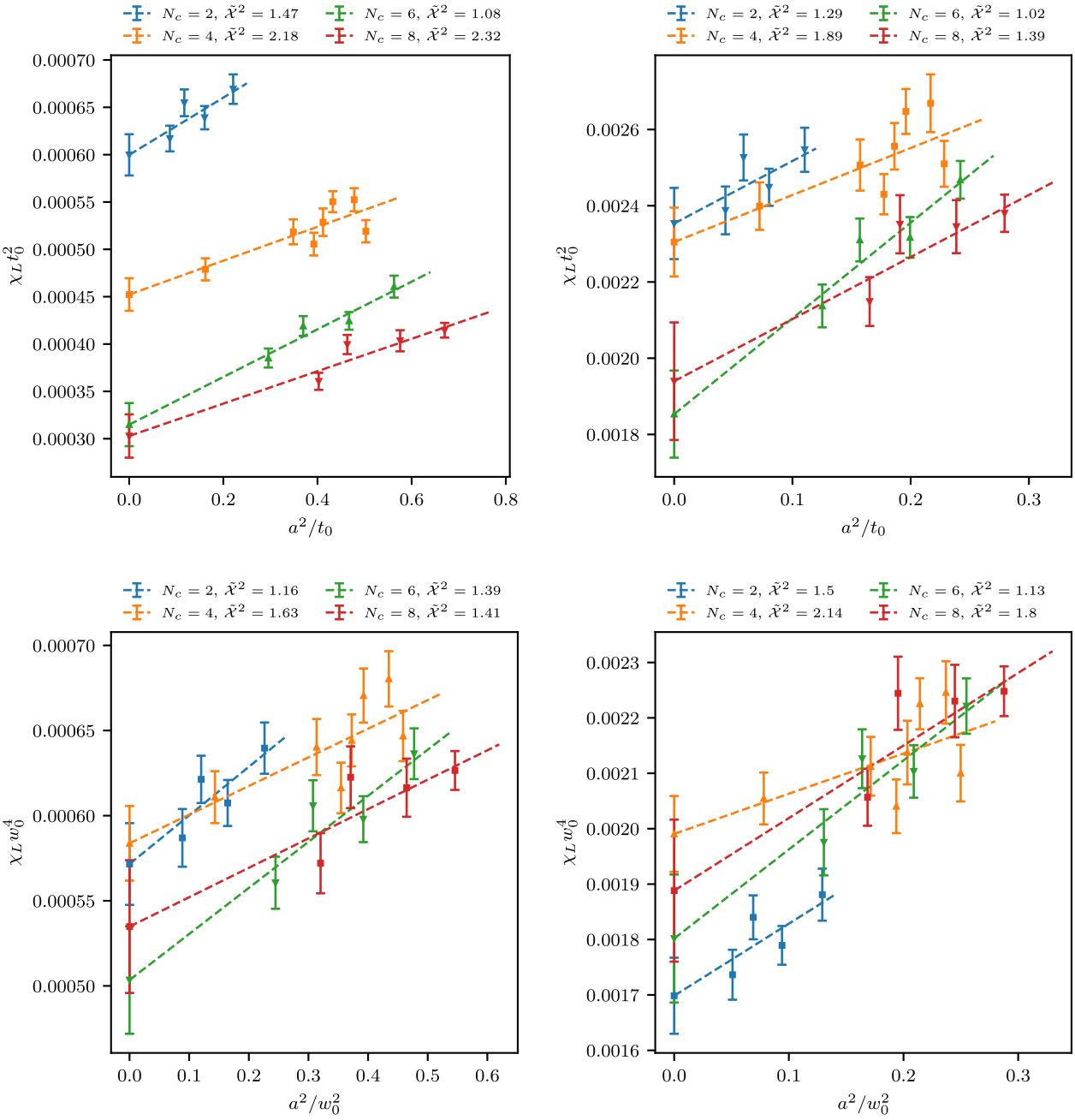

FIG. 11. Topological susceptibility per unit volume $\chi_L t_0^2$ as a function of a^2/t_0 (top panels) and $\chi_L w_0^4$ as a function of a^2/w_0^2 (bottom), in $Sp(N_c)$ Yang-Mills theories with $N_c = 2, 4, 6, 8$. We adopt reference values $c_e = c_w = 0.225$ (left panels) and $c_e = c_w = 0.5$ (right). Our continuum extrapolations are represented as dashed lines. The results are reported in Table VI.

$$\chi_L(a)t_0^2 = \chi_L(a=0)t_0^2 + c_1\frac{a^2}{t_0}, \tag{36}$$

for each value of N_c, separately. The results of this extrapolation are reported in Table VI (and displayed in Fig. 11) for $c_e = 0.225$ and $c_e = 0.5$, respectively. For completeness, we also report in the same Table VI and Fig. 11 also the extrapolation of $\chi_L w_0^2$, obtained with a similar fitting function which includes one correction term $\mathcal{O}(\frac{a^2}{w_0^2})$. The uncertainty on the extrapolated values are obtained from the maximum likelihood analysis by including statistical uncertainties only. Reference [65], which reports χt_0^2 for $SU(N_c)$ with $N_c = 3, 4, 5, 6$, present the results in units of t_0, and for the choice $c_e = 0.225$. Unfortunately, a direct comparison is not possible, as the authors of Ref. [65] did not report on the common $SU(2) \sim Sp(2)$ case. We will return to the comparison of the topological susceptibility in $Sp(N_c)$ and $SU(N_c)$ theories in a companion publication [75].

V. SUMMARY AND DISCUSSION

We studied the four-dimensional Yang-Mills theories with group $Sp(N_c)$, for $N_c = 2, 4, 6, 8$, by means of lattice numerical techniques. We used the Wilson flow as a scale-setting procedure. We showed that lattice artifacts are reduced by adopting the clover-leaf plaquette discretization. We also found that by simultaneously rescaling $\mathcal{E}(t)$ [or alternatively $\mathcal{W}(t)$], the reference value of $\mathcal{E}_0$ (or alternatively $\mathcal{W}_0$), and t_0/a^2 (or alternatively w_0/a), the Wilson flows for different gauge groups agree (within numerical errors) over a nontrivial range of t. The proposed rescaling is based upon the group-factor dependence of the leading-order perturbative evaluation of $\mathcal{E}(t)$, indicating that the suppression of subleading corrections that differentiate the groups holds also nonperturbatively, over a finite range of flow time t.

We then computed the topological susceptibility from our lattice ensembles, expressed it in units of the Wilson flow scale t_0 (w_0), and performed the continuum extrapolation for the four gauge groups. We summarize in Table VI our results for the continuum extrapolation of χt_0^2 and χw_0^4 for two different choices of reference values for $\mathcal{E}_0$ and $\mathcal{W}_0$. In a companion paper [75], we present our extrapolation of the measurement of the topological susceptibility towards the large-N_c limit (in units of the string tension), and discuss how to compare it with the analogous calculations performed for $SU(N_c)$ Yang-Mills theories.

All data presented, as well as underlying raw data, are available at Ref. [88], and the analysis code used to prepare the main figures and tables are shared at Ref. [89].

ACKNOWLEDGMENTS

The work of E. B. has been funded in part by the Supercomputing Wales project, which is part-funded by the European Regional Development Fund (ERDF) via Welsh Government, and by the UKRI Science and Technology Facilities Council (STFC) Research Software Engineering Fellowship No. EP/V052489/1. The work of D. K. H. was supported by the National Research Foundation of Korea (NRF) grant funded by the Korea government (MSIT) (2021R1A4A5031460) and also by Basic Science Research Program through the National Research Foundation of Korea (NRF) funded by the Ministry of Education (NRF-2017R1D1A1B06033701). The work of J.-W. L. is supported by the National Research Foundation of Korea (NRF) grant funded by the Korea government (MSIT) (NRF-2018R1C1B3001379). The work of C.-J. D. L. is supported by the Taiwanese MoST Grant No. 109-2112-M-009-006-MY3. The work of B. L. and M. P. has been supported in part by the STFC Consolidated Grants No. ST/P00055X/1 and No. ST/T000813/1. B. L. and M. P. received funding from the European Research Council (ERC) under the European Union's Horizon 2020 research and innovation program under Grant Agreement No. 813942. The work of B. L. is further supported in part by the Royal Society Wolfson Research Merit Grant No. WM170010 and by the Leverhulme Trust Research Fellowship No. RF-2020-4619. The work of D. V., is supported in part by the INFN HPC-HTC project and in part by the Simons Foundation under the program "Targeted Grants to Institutes" awarded to the Hamilton Mathematics Institute. Numerical simulations have been performed on the Swansea University SUNBIRD cluster (part of the Supercomputing Wales project) and AccelerateAI A100 GPU system, on the local HPC clusters in Pusan National University (PNU) and in National Yang Ming Chiao Tung University (NYCU), and the DiRAC Data Intensive service at Leicester. The Swansea University SUNBIRD system and AccelerateAI are part funded by the European Regional Development Fund (ERDF) via Welsh Government. The DiRAC Data Intensive service at Leicester is operated by the University of Leicester IT Services, which forms part of the STFC DiRAC HPC Facility (www.dirac.ac.uk). The DiRAC Data Intensive service equipment at Leicester was funded by BEIS capital funding via STFC capital Grants No. ST/K000373/1 and No. ST/R002363/1 and STFC DiRAC Operations Grant No. ST/R001014/1. DiRAC is part of the National e-Infrastructure.

APPENDIX: SCALE-SETTING DATA FOR $N_c = 2, 4, 8$

In this appendix, we report the intermediate results of the scale-setting procedure for the $Sp(2)$, $Sp(4)$, and $Sp(8)$

TABLE VII. The gradient flow scale $\sqrt{t_0}/a$ for different choices of $\mathcal{E}_0$ and β, for $N_c = 2$. We report the results for both the plaquette and clover discretizations.

β	$\mathcal{E}_0$	$\sqrt{t_0}/a$ (pl.)	$\sqrt{t_0}/a$ (cl.)
2.55	0.3	2.6989(30)	2.7489(29)
2.60	0.3	3.1810(33)	3.2244(32)
2.65	0.3	3.7340(29)	3.7714(30)
2.70	0.3	4.3570(48)	4.3900(46)
2.55	0.4	3.0384(36)	3.0883(34)
2.60	0.4	3.5774(40)	3.6209(38)
2.65	0.4	4.1958(36)	4.2335(36)
2.70	0.4	4.8929(57)	4.9263(55)
2.55	0.5	3.3189(41)	3.3694(40)
2.60	0.5	3.9040(46)	3.9484(43)
2.65	0.5	4.5761(41)	4.6146(41)
2.70	0.5	5.3333(66)	5.3680(64)
2.55	0.6	3.5614(47)	3.6131(45)
2.60	0.6	4.1864(51)	4.2320(48)
2.65	0.6	4.9040(46)	4.9438(46)
2.70	0.6	⋯	⋯

TABLE VIII. The gradient flow scale w_0/a for different choices of $\mathcal{W}_0$ as a function of β, for $N_c = 2$. We report the results for both the plaquette and clover discretizations.

β	$\mathcal{W}_0$	w_0/a (pl.)	w_0/a (cl.)
2.55	0.3	1.5961(11)	1.6046(10)
2.60	0.3	1.7292(11)	1.7366(10)
2.65	0.3	1.87188(92)	1.87785(90)
2.70	0.3	2.0210(14)	2.0260(13)
2.55	0.4	1.6776(12)	1.6868(11)
2.60	0.4	1.8185(13)	1.8260(12)
2.65	0.4	1.9669(10)	1.9732(10)
2.70	0.4	2.1235(16)	2.1287(15)
2.55	0.5	1.7448(13)	1.7541(13)
2.60	0.5	1.8889(14)	1.8973(13)
2.65	0.5	2.0435(11)	2.0502(11)
2.70	0.5	2.2045(18)	2.2102(16)
2.55	0.6	1.8002(15)	1.8104(14)
2.60	0.6	1.9487(14)	1.9576(14)
2.65	0.6	2.1082(13)	2.1151(12)
2.70	0.6	...	...

TABLE IX. The gradient flow scale $\sqrt{t_0}/a$ for different choices of $\mathcal{E}_0$ and β, for $N_c = 4$. We report the results for both the plaquette and clover discretizations.

β	$\mathcal{E}_0$	$\sqrt{t_0}/a$ (pl.)	$\sqrt{t_0}/a$ (cl.)
7.7	0.3	1.37620(40)	1.46197(40)
7.72	0.3	1.41690(43)	1.49953(42)
7.76	0.3	1.49948(50)	1.57652(50)
7.78	0.3	1.54145(54)	1.61595(53)
7.80	0.3	1.58361(60)	1.65573(57)
7.85	0.3	1.68978(70)	1.75659(67)
7.7	0.4	1.62985(53)	1.69845(52)
7.72	0.4	1.67629(55)	1.74253(55)
7.76	0.4	1.77067(65)	1.83274(65)
7.78	0.4	1.81913(70)	1.87920(70)
7.80	0.4	1.86744(78)	1.92574(75)
7.85	0.4	1.99001(92)	2.04422(88)
7.7	0.5	1.82938(63)	1.89073(62)
7.72	0.5	1.88069(66)	1.94002(66)
7.76	0.5	1.98496(78)	2.04067(77)
7.78	0.5	2.03884(84)	2.09278(84)
7.80	0.5	2.09229(94)	2.14469(91)
7.85	0.5	2.2286(11)	2.2774(11)
7.7	0.6	1.99738(73)	2.05499(71)
7.72	0.6	2.05290(76)	2.10871(76)
7.76	0.6	2.16562(90)	2.21813(89)
7.78	0.6	2.22422(97)	2.27504(97)
7.80	0.6	2.2821(11)	2.3315(10)
7.85	0.6	2.4302(13)	2.4762(12)

TABLE X. The gradient flow scale w_0/a for different choices of $\mathcal{W}_0$ as a function of β, for $N_c = 4$. We report the results for both the plaquette and clover discretizations.

β	$\mathcal{W}_0$	w_0/a (pl.)	w_0/a (cl.)
7.7	0.3	1.22784(24)	1.23049(24)
7.72	0.3	1.24453(25)	1.24707(25)
7.76	0.3	1.27680(29)	1.27933(28)
7.78	0.3	1.29372(31)	1.29613(30)
7.80	0.3	1.30975(34)	1.31216(32)
7.85	0.3	1.35073(39)	1.35299(37)
7.7	0.4	1.29494(27)	1.30037(27)
7.72	0.4	1.31252(28)	1.31777(28)
7.76	0.4	1.34674(33)	1.35169(32)
7.78	0.4	1.36470(35)	1.36940(34)
7.80	0.4	1.38167(38)	1.38628(37)
7.85	0.4	1.42523(44)	1.42944(42)
7.7	0.5	1.34954(30)	1.35640(29)
7.72	0.5	1.36784(31)	1.37449(30)
7.76	0.5	1.40345(36)	1.40970(35)
7.78	0.5	1.42221(38)	1.42816(38)
7.80	0.5	1.43994(41)	1.44572(40)
7.85	0.5	1.48552(49)	1.49076(47)
7.7	0.6	1.39593(33)	1.40365(32)
7.72	0.6	1.41485(33)	1.42232(33)
7.76	0.6	1.45159(39)	1.45864(38)
7.78	0.6	1.47110(42)	1.47776(41)
7.80	0.6	1.48942(44)	1.49585(44)
7.85	0.6	1.53659(53)	1.54244(51)

TABLE XI. The gradient flow scale $\sqrt{t_0}/a$ for different choices of $\mathcal{E}_0$ and β, for $N_c = 8$. We report the results for both the plaquette and clover discretizations.

β	$\mathcal{E}_0$	$\sqrt{t_0}/a$ (pl.)	$\sqrt{t_0}/a$ (cl.)
26.5	0.3	...	...
26.7	0.3	...	...
27.0	0.3	...	...
27.2	0.3	...	...
26.5	0.4	0.6428(11)	1.04083(17)
26.7	0.4	0.91955(26)	1.12079(20)
27.0	0.4	1.09768(30)	1.24650(27)
27.2	0.4	1.20530(34)	1.33540(35)
26.5	0.5	1.08015(25)	1.21190(23)
26.7	0.5	1.19344(27)	1.30764(27)
27.0	0.5	1.36119(40)	1.45737(38)
27.2	0.5	1.47602(46)	1.56329(49)
26.5	0.6	1.25801(30)	1.35615(28)
26.7	0.6	1.37719(33)	1.46475(34)
27.0	0.6	1.55864(49)	1.63417(47)
27.2	0.6	1.68496(57)	1.75412(61)

TABLE XII. The gradient flow scale w_0/a for different choices of $\mathcal{W}_0$ as a function of β, for $N_c = 8$. We report the results for both the plaquette and clover discretizations.

β	$\mathcal{W}_0$	w_0/a (pl.)	w_0/a (cl.)
26.5	0.3	⋯	⋯
26.7	0.3	⋯	⋯
27.0	0.3	⋯	⋯
27.2	0.3	⋯	⋯
26.5	0.4	1.11790(16)	1.10726(15)
26.7	0.4	1.16124(17)	1.15275(18)
27.0	0.4	1.22617(25)	1.21983(24)
27.2	0.4	1.27059(28)	1.26524(30)
26.5	0.5	1.16496(18)	1.16048(17)
26.7	0.5	1.21151(19)	1.20807(20)
27.0	0.5	1.28068(28)	1.27826(27)
27.2	0.5	1.32779(31)	1.32582(34)
26.5	0.6	1.20570(19)	1.20466(18)
26.7	0.6	1.25467(21)	1.25407(22)
27.0	0.6	1.32710(31)	1.32690(29)
27.2	0.6	1.37632(34)	1.37627(37)

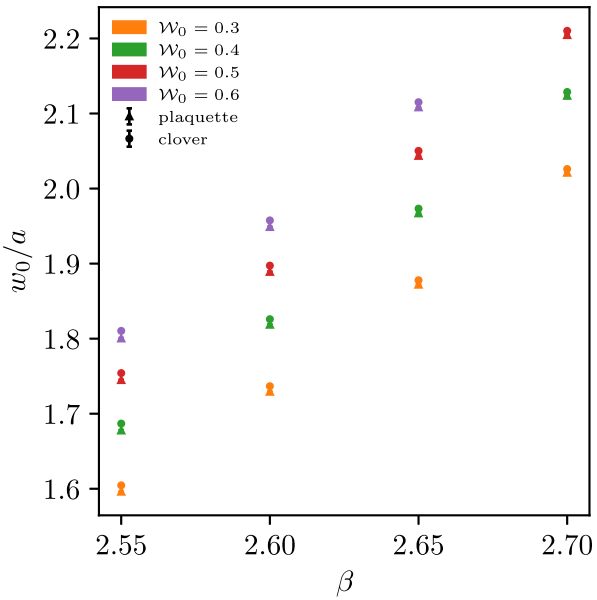

FIG. 13. The gradient flow scale w_0/a in $Sp(2)$, for different choices of $\mathcal{W}_0$, as a function of β, and comparing plaquette and clover discretization.

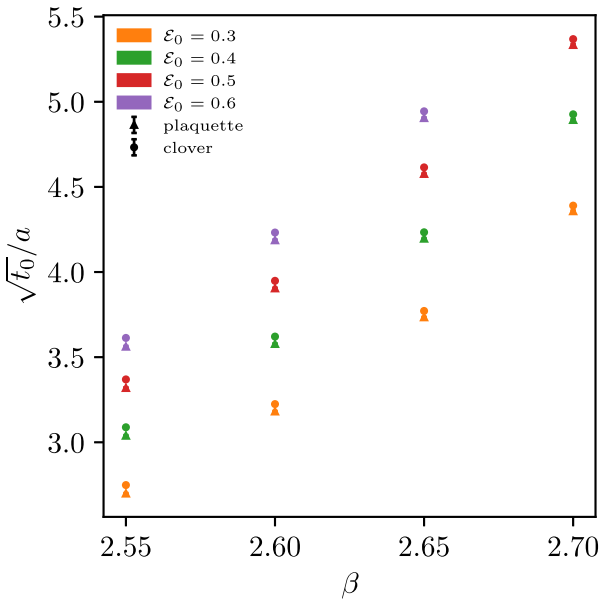

FIG. 12. The gradient flow scale $\sqrt{t_0}/a$ in $Sp(2)$, for different choices of $\mathcal{E}_0$, as a function of β, and comparing plaquette and clover discretization.

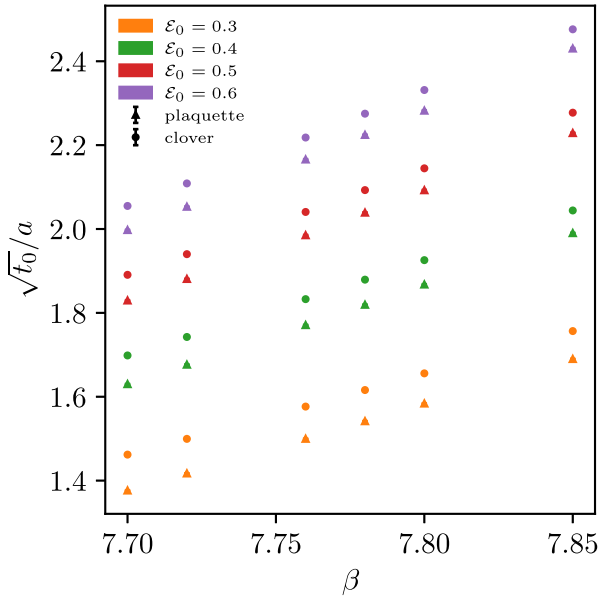

FIG. 14. The gradient flow scale $\sqrt{t_0}/a$ in $Sp(4)$, for different choices of $\mathcal{E}_0$, as a function of β, and comparing plaquette and clover discretization.

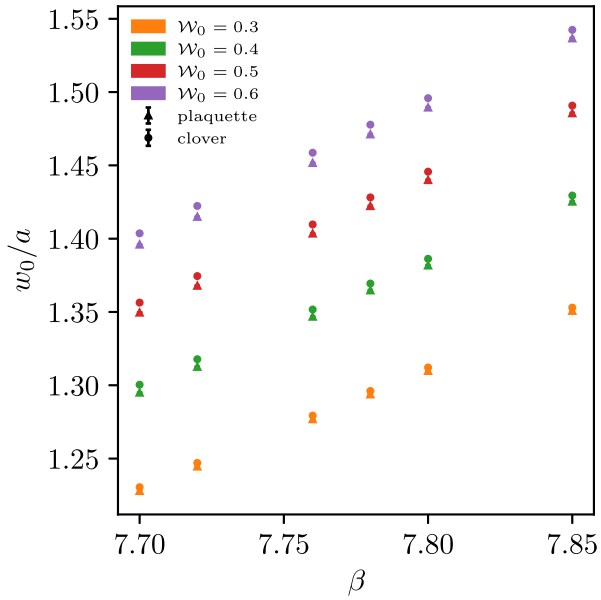

FIG. 15. The gradient flow scale w_0/a in $Sp(4)$, for different choices of $\mathcal{W}_0$, as a function of β, and comparing plaquette and clover discretization.

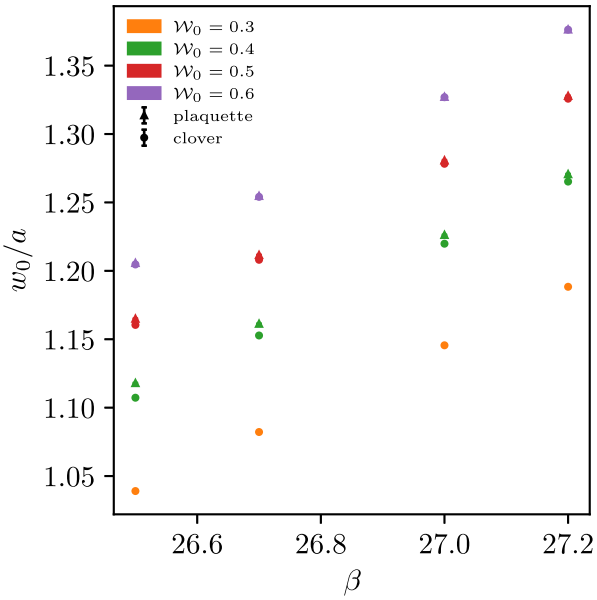

FIG. 17. The gradient flow scale w_0/a in $Sp(8)$, for different choices of $\mathcal{W}_0$, as a function of β, and comparing plaquette and clover discretization.

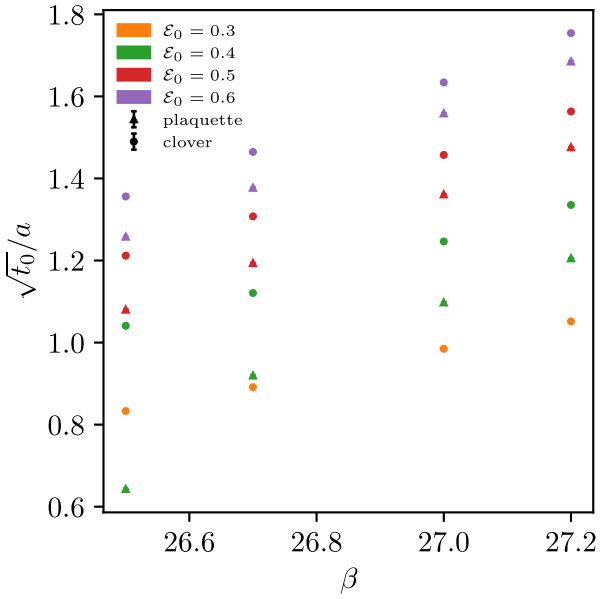

FIG. 16. The gradient flow scale $\sqrt{t_0}/a$ in $Sp(8)$, for different choices of $\mathcal{E}_0$, as a function of β, and comparing plaquette and clover discretization.

Yang-Mills theories. The presentation mirrors the one for the $Sp(6)$ theory, in the main body of the paper. Tables VII and VIII present our results for t_0/a^2 and w_0/a, respectively, for various choices of reference values $\mathcal{E}_0$ and $\mathcal{W}_0$, for $N_c = 2$. We tabulate the results for both the plaquette and clover discretizations. Tables IX and X list the same information, but for $Sp(4)$, while Tables XI and XII refer to $Sp(8)$. Cases in which Eqs. (24) or (26) do not admit a solution, because of extreme choices of $\mathcal{E}_0$ or $\mathcal{W}_0$, are left blank. The information in Tables VII–XII is also graphically displayed in Figs. 12–17, and available in machine-readable form in Ref. [88].

[1] A. Hietanen, R. Lewis, C. Pica, and F. Sannino, Fundamental composite Higgs dynamics on the lattice: SU(2) with two flavors, J. High Energy Phys. 07 (2014) 116.

[2] W. Detmold, M. McCullough, and A. Pochinsky, Dark nuclei. II. Nuclear spectroscopy in two-color QCD, Phys. Rev. D **90**, 114506 (2014).

[3] R. Arthur, V. Drach, M. Hansen, A. Hietanen, C. Pica, and F. Sannino, SU(2) gauge theory with two fundamental flavors: A minimal template for model building, Phys. Rev. D **94**, 094507 (2016).

[4] R. Arthur, V. Drach, A. Hietanen, C. Pica, and F. Sannino, $SU(2)$ gauge theory with two fundamental flavours: Scalar and pseudoscalar spectrum, arXiv:1607.06654.

[5] C. Pica, V. Drach, M. Hansen, and F. Sannino, Composite Higgs dynamics on the lattice, EPJ Web Conf. **137**, 10005 (2017).

[6] J. W. Lee, B. Lucini, and M. Piai, Symmetry restoration at high-temperature in two-color and two-flavor lattice gauge theories, J. High Energy Phys. 04 (2017) 036.

[7] V. Drach, T. Janowski, and C. Pica, Update on SU(2) gauge theory with NF $= 2$ fundamental flavours, EPJ Web Conf. **175**, 08020 (2018).

[8] V. Drach, T. Janowski, C. Pica, and S. Prelovsek, Scattering of goldstone bosons and resonance production in a composite Higgs model on the lattice, J. High Energy Phys. 04 (2021) 117.

[9] V. Drach, P. Fritzsch, A. Rago, and F. Romero-López, Singlet channel scattering in a composite Higgs model on the lattice, Eur. Phys. J. C **82**, 47 (2022).

[10] E. Bennett, D. K. Hong, J. W. Lee, C.-J. D. Lin, B. Lucini, M. Piai, and D. Vadacchino, Sp(4) gauge theory on the lattice: Towards SU(4)/Sp(4) composite Higgs (and beyond), J. High Energy Phys. 03 (2018) 185.

[11] J. W. Lee, E. Bennett, D. K. Hong, C. J. D. Lin, B. Lucini, M. Piai, and D. Vadacchino, Progress in the lattice simulations of Sp($2N$) gauge theories, Proc. Sci. LATTICE2018 (**2018**) 192 [arXiv:1811.00276].

[12] E. Bennett, D. K. Hong, J. W. Lee, C. J. D. Lin, B. Lucini, M. Piai, and D. Vadacchino, Sp(4) gauge theories on the lattice: $N_f = 2$ dynamical fundamental fermions, J. High Energy Phys. 12 (2019) 053.

[13] E. Bennett, D. K. Hong, J. W. Lee, C. J. D. Lin, B. Lucini, M. Mesiti, M. Piai, J. Rantaharju, and D. Vadacchino, $Sp(4)$ gauge theories on the lattice: Quenched fundamental and antisymmetric fermions, Phys. Rev. D **101**, 074516 (2020).

[14] E. Bennett, J. Holligan, D. K. Hong, J. W. Lee, C. J. D. Lin, B. Lucini, M. Piai, and D. Vadacchino, Color dependence of tensor and scalar glueball masses in Yang-Mills theories, Phys. Rev. D **102**, 011501 (2020).

[15] E. Bennett, J. Holligan, D. K. Hong, J. W. Lee, C. J. D. Lin, B. Lucini, M. Piai, and D. Vadacchino, Glueballs and strings in $Sp(2N)$ Yang-Mills theories, Phys. Rev. D **103**, 054509 (2021).

[16] E. Bennett, D. K. Hong, H. Hsiao, J. W. Lee, C. J. D. Lin, B. Lucini, M. Mesiti, M. Piai, and D. Vadacchino, Lattice studies of the $Sp(4)$ gauge theory with two fundamental and three antisymmetric Dirac fermions, Phys. Rev. D **106**, 014501 (2022).

[17] E. Bennett, D. K. Hong, H. Hsiao, J. W. Lee, C. J. D. Lin, B. Lucini, M. Piai, and D. Vadacchino, Sp(4) theories on the lattice: Dynamical antisymmetric fermions (to be published).

[18] J. Barnard, T. Gherghetta, and T. S. Ray, UV descriptions of composite Higgs models without elementary scalars, J. High Energy Phys. 02 (2014) 002.

[19] D. B. Kaplan and H. Georgi, SU(2) × U(1) breaking by vacuum misalignment, Phys. Lett. **136B**, 183 (1984).

[20] H. Georgi and D. B. Kaplan, Composite Higgs and custodial SU(2), Phys. Lett. **145B**, 216 (1984).

[21] M. J. Dugan, H. Georgi, and D. B. Kaplan, Anatomy of a composite Higgs model, Nucl. Phys. **B254**, 299 (1985).

[22] D. B. Kaplan, Flavor at SSC energies: A new mechanism for dynamically generated fermion masses, Nucl. Phys. **B365**, 259 (1991).

[23] G. Panico and A. Wulzer, The composite Nambu-Goldstone Higgs, Lect. Notes Phys. **913**, 1 (2016).

[24] O. Witzel, Review on composite Higgs models, Proc. Sci. LATTICE2018 (**2019**) 006 [arXiv:1901.08216].

[25] G. Cacciapaglia, C. Pica, and F. Sannino, Fundamental composite dynamics: A review, Phys. Rep. **877**, 1 (2020).

[26] G. Ferretti and D. Karateev, Fermionic UV completions of composite Higgs models, J. High Energy Phys. 03 (2014) 077.

[27] G. Ferretti, Gauge theories of partial compositeness: Scenarios for Run-II of the LHC, J. High Energy Phys. 06 (2016) 107.

[28] G. Cacciapaglia, G. Ferretti, T. Flacke, and H. Serôdio, Light scalars in composite Higgs models, Front. Phys. **7**, 22 (2019).

[29] Y. Hochberg, E. Kuflik, T. Volansky, and J. G. Wacker, Mechanism for Thermal Relic Dark Matter of Strongly Interacting Massive Particles, Phys. Rev. Lett. **113**, 171301 (2014).

[30] Y. Hochberg, E. Kuflik, H. Murayama, T. Volansky, and J. G. Wacker, Model for Thermal Relic Dark Matter of Strongly Interacting Massive Particles, Phys. Rev. Lett. **115**, 021301 (2015).

[31] Y. Hochberg, E. Kuflik, and H. Murayama, SIMP spectroscopy, J. High Energy Phys. 05 (2016) 090.

[32] D. Kondo, R. McGehee, T. Melia, and H. Murayama, Linear sigma dark matter, J. High Energy Phys. 09 (2022) 041.

[33] N. Bernal, X. Chu, and J. Pradler, Simply split strongly interacting massive particles, Phys. Rev. D **95**, 115023 (2017).

[34] A. Berlin, N. Blinov, S. Gori, P. Schuster, and N. Toro, Cosmology and accelerator tests of strongly interacting dark matter, Phys. Rev. D **97**, 055033 (2018).

[35] N. Bernal, X. Chu, S. Kulkarni, and J. Pradler, Self-interacting dark matter without prejudice, Phys. Rev. D **101**, 055044 (2020).

[36] H. Cai and G. Cacciapaglia, Singlet dark matter in the SU(6)/SO(6) composite Higgs model, Phys. Rev. D **103**, 055002 (2021).

[37] Y. D. Tsai, R. McGehee, and H. Murayama, Resonant Self-Interacting Dark Matter from Dark QCD, Phys. Rev. Lett. **128**, 172001 (2022).

[38] A. Maas and F. Zierler, Strong isospin breaking in Sp(4) gauge theory, Proc. Sci. LATTICE2021 (**2022**) 130 [arXiv:2109.14377].

[39] F. Zierler and A. Maas, $Sp(4)$ SIMP dark matter on the lattice, Proc. Sci. LHCP2021 (**2021**) 162, https://pos.sissa.it/397/162/pdf.

[40] S. Kulkarni, A. Maas, S. Mee, M. Nikolic, J. Pradler, and F. Zierler, Low-energy effective description of dark $Sp(4)$ theories, arXiv:2202.05191.

[41] K. Holland, M. Pepe, and U. J. Wiese, The deconfinement phase transition of Sp(2) and Sp(3) Yang-Mills theories in $(2+1)$-dimensions and $(3+1)$-dimensions, Nucl. Phys. **B694**, 35 (2004).

[42] J. M. Maldacena, The large N limit of superconformal field theories and supergravity, Int. J. Theor. Phys. **38**, 1113 (1999); Adv. Theor. Math. Phys. **2**, 231 (1998).

[43] S. S. Gubser, I. R. Klebanov, and A. M. Polyakov, Gauge theory correlators from noncritical string theory, Phys. Lett. B **428**, 105 (1998).

[44] E. Witten, Anti-de Sitter space and holography, Adv. Theor. Math. Phys. **2**, 253 (1998).

[45] O. Aharony, S. S. Gubser, J. M. Maldacena, H. Ooguri, and Y. Oz, Large N field theories, string theory and gravity, Phys. Rep. **323**, 183 (2000).

[46] B. Lucini and M. Teper, SU(N) gauge theories in four-dimensions: Exploring the approach to N = infinity, J. High Energy Phys. 06 (2001) 050.

[47] B. Lucini, M. Teper, and U. Wenger, Glueballs and k-strings in SU(N) gauge theories: Calculations with improved operators, J. High Energy Phys. 06 (2004) 012.

[48] B. Lucini, A. Rago, and E. Rinaldi, Glueball masses in the large N limit, J. High Energy Phys. 08 (2010) 119.

[49] B. Lucini and M. Panero, SU(N) gauge theories at large N, Phys. Rep. **526**, 93 (2013).

[50] A. Athenodorou, R. Lau, and M. Teper, On the weak N -dependence of SO(N) and SU(N) gauge theories in $2+1$ dimensions, Phys. Lett. B **749**, 448 (2015).

[51] R. Lau and M. Teper, SO(N) gauge theories in $2+1$ dimensions: Glueball spectra and confinement, J. High Energy Phys. 10 (2017) 022.

[52] D. K. Hong, J. W. Lee, B. Lucini, M. Piai, and D. Vadacchino, Casimir scaling and Yang–Mills glueballs, Phys. Lett. B **775**, 89 (2017).

[53] N. Yamanaka, A. Nakamura, and M. Wakayama, Interglueball potential in lattice SU(N) gauge theories, *Proc. Sci.* LATTICE2021 (2022) 447 [arXiv:2110.04521].

[54] P. Hernández and F. Romero-López, The large N_c limit of QCD on the lattice, Eur. Phys. J. A **57**, 52 (2021).

[55] A. Athenodorou and M. Teper, SU(N) gauge theories in $3+1$ dimensions: Glueball spectrum, string tensions and topology, J. High Energy Phys. 12 (2021) 082.

[56] C. Bonanno, M. D'Elia, B. Lucini, and D. Vadacchino, Towards glueball masses of large-N $\mathrm{SU}(N)$ pure-gauge theories without topological freezing, Phys. Lett. B **833**, 137281 (2022).

[57] E. Witten, Current algebra theorems for the U(1) goldstone boson, Nucl. Phys. **B156**, 269 (1979).

[58] G. Veneziano, U(1) without instantons, Nucl. Phys. **B159**, 213 (1979).

[59] L. Del Debbio, H. Panagopoulos, and E. Vicari, θ dependence of SU(N) gauge theories, J. High Energy Phys. 08 (2002) 044.

[60] B. Lucini, M. Teper, and U. Wenger, Topology of SU(N) gauge theories at T = ~0 and T = ~T(c), Nucl. Phys. **B715**, 461 (2005).

[61] L. Del Debbio, L. Giusti, and C. Pica, Topological Susceptibility in the SU(3) Gauge Theory, Phys. Rev. Lett. **94**, 032003 (2005).

[62] M. Luscher and F. Palombi, Universality of the topological susceptibility in the SU(3) gauge theory, J. High Energy Phys. 09 (2010) 110.

[63] H. Panagopoulos and E. Vicari, The 4D SU(3) gauge theory with an imaginary θ term, J. High Energy Phys. 11 (2011) 119.

[64] C. Bonati, M. D'Elia, and A. Scapellato, θ dependence in $SU(3)$ Yang-Mills theory from analytic continuation, Phys. Rev. D **93**, 025028 (2016).

[65] M. Cè and M. García Vera, L. Giusti, and S. Schaefer, The topological susceptibility in the large-N limit of $\mathrm{SU}(N)$ Yang–Mills theory, Phys. Lett. B **762**, 232 (2016).

[66] C. Bonati, M. D'Elia, P. Rossi, and E. Vicari, θ dependence of 4D $SU(N)$ gauge theories in the large-N limit, Phys. Rev. D **94**, 085017 (2016).

[67] C. Alexandrou, A. Athenodorou, K. Cichy, A. Dromard, E. Garcia-Ramos, K. Jansen, U. Wenger, and F. Zimmermann, Comparison of topological charge definitions in lattice QCD, Eur. Phys. J. C **80**, 424 (2020).

[68] C. Bonanno, C. Bonati, and M. D'Elia, Large-N $SU(N)$ Yang-Mills theories with milder topological freezing, J. High Energy Phys. 03 (2021) 111.

[69] S. Borsanyi and D. Sexty, Topological susceptibility of pure gauge theory using Density of States, Phys. Lett. B **815**, 136148 (2021).

[70] G. Cossu, D. Lancastera, B. Lucini, R. Pellegrini, and A. Rago, Ergodic sampling of the topological charge using the density of states, Eur. Phys. J. C **81**, 375 (2021).

[71] M. Teper, More methods for calculating the topological charge (density) of SU(N) lattice gauge fields in $3+1$ dimensions, arXiv:2202.02528.

[72] E. Vicari and H. Panagopoulos, θ dependence of SU(N) gauge theories in the presence of a topological term, Phys. Rep. **470**, 93 (2009).

[73] B. Lucini, E. Bennett, J. Holligan, D. K. Hong, H. Hsiao, J. W. Lee, C. J. D. Lin, M. Mesiti, M. Piai, and D. Vadacchino, Sp(4) gauge theories and beyond the standard model physics, EPJ Web Conf. **258**, 08003 (2022).

[74] E. Bennett, J. Holligan, D. K. Hong, H. Hsiao, J. W. Lee, C. J. D. Lin, B. Lucini, M. Mesiti, M. Piai, and D. Vadacchino, Progress in $Sp(2N)$ lattice gauge theories, Proc. Sci. LATTICE2021 (**2022**) 308 [arXiv:2111.14544].

[75] E. Bennett, D. K. Hong, J. W. Lee, C. J. D. Lin, B. Lucini, M. Piai, and D. Vadacchino, Color dependence of the topological susceptibility in Yang-Mills theories, arXiv:2205.09254.

[76] M. Lüscher, Properties and uses of the Wilson flow in lattice QCD, J. High Energy Phys. 08 (2010) 071; 03 (2014) 092(E).

[77] M. Lüscher, Future applications of the Yang-Mills gradient flow in lattice QCD, Proc. Sci. LATTICE2013 (**2014**) 016 [arXiv:1308.5598].

[78] B. Sheikholeslami and R. Wohlert, Improved continuum limit lattice action for QCD with wilson fermions, Nucl. Phys. **B259**, 572 (1985).
[79] M. Hasenbusch and K. Jansen, Speeding up lattice QCD simulations with clover improved Wilson fermions, Nucl. Phys. **B659**, 299 (2003).
[80] https://github.com/sa2c/HiRep.
[81] L. Del Debbio, A. Patella, and C. Pica, Higher representations on the lattice: Numerical simulations. SU(2) with adjoint fermions, Phys. Rev. D **81**, 094503 (2010).
[82] M. Campostrini, A. Di Giacomo, H. Panagopoulos, and E. Vicari, Topological charge, renormalization and cooling on the lattice, Nucl. Phys. **B329**, 683 (1990).
[83] M. Luscher, Topology of lattice gauge fields, Commun. Math. Phys. **85**, 39 (1982).
[84] M. Luscher and S. Schaefer, Lattice QCD without topology barriers, J. High Energy Phys. 07 (2011) 036.
[85] M. G. Endres, R. C. Brower, W. Detmold, K. Orginos, and A. V. Pochinsky, Multiscale Monte Carlo equilibration: Pure Yang-Mills theory, Phys. Rev. D **92**, 114516 (2015).
[86] M. Lüscher, Stochastic locality and master-field simulations of very large lattices, EPJ Web Conf. **175**, 01002 (2018).
[87] S. Borsanyi, S. Durr, Z. Fodor, C. Hoelbling, S. D. Katz, S. Krieg, T. Kurth, L. Lellouch, T. Lippert, C. McNeile *et al.*, High-precision scale setting in lattice QCD, J. High Energy Phys. 09 (2012) 010.
[88] E. Bennett, D. K. Hong, J. W. Lee, C. J. D. Lin, B. Lucini, M. Piai, and D. Vadacchino, $Sp(2N)$ Yang-Mills theories on the lattice: Scale setting and topology-data release, 10.5281/zenodo.6678411 (2022).
[89] E. Bennett, D. K. Hong, J. W. Lee, C. J. D. Lin, B. Lucini, M. Piai, and D. Vadacchino, $Sp(2N)$ Yang-Mills theories on the lattice: Scale setting and topology-analysis workflow, 10.5281/zenodo.6685967 (2022).
[90] N. Madras and A. D. Sokal, The Pivot algorithm: A highly efficient Monte Carlo method for self-avoiding walk, J. Stat. Phys. **50**, 109 (1988).